Cell Reports
Medicine

Article

Tissue-resident memory CAR T cells with stem-like characteristics display enhanced efficacy against solid and liquid tumors

Graphical abstract

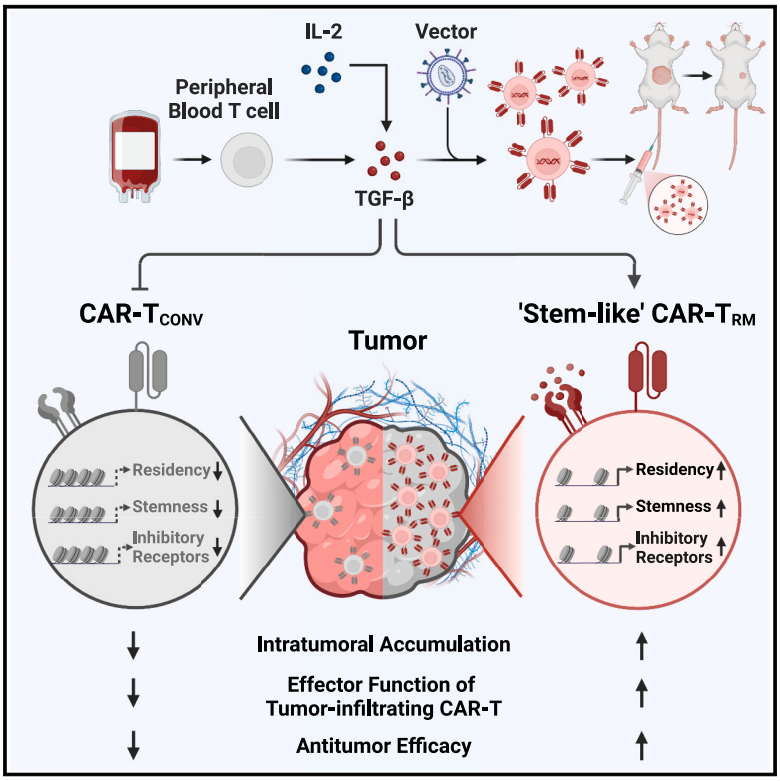

Highlights

- TGF-β induces CAR-T$_{RM}$ cells with enhanced tumor infiltration
- Chromatin changes via TGF-β create a stem-like resident memory fate
- CAR-T$_{RM}$ cells resist tumor-imposed dysfunction
- CAR-T$_{RM}$ cells show potent efficacy in solid and liquid cancers

Authors

In-Young Jung, Estela Noguera-Ortega, Robert Bartoszek, ..., Edmund K. Moon, Steven M. Albelda, Joseph A. Fraietta

Correspondence

jfrai@upenn.edu

In brief

CAR T cells exhibit promise in cancer immunotherapy. Jung et al. show that combining CAR engineering with TGF-β exposure in *ex vivo* blood T cells enhances stem-like properties and tissue residency, which is linked to chromatin and transcriptional changes. This results in improved tumor infiltration and enhanced efficacy in various cancer models.

Jung et al., 2023, Cell Reports Medicine *4*, 101053
June 20, 2023
https://doi.org/10.1016/j.xcrm.2023.101053

CellPress

Cell Reports Medicine

CellPress
OPEN ACCESS

Article

Tissue-resident memory CAR T cells with stem-like characteristics display enhanced efficacy against solid and liquid tumors

In-Young Jung,[1,2,3,4] Estela Noguera-Ortega,[2,3,5] Robert Bartoszek,[1,2,3,4] Sierra M. Collins,[6,7,8,9] Erik Williams,[1,2,3,4] Megan Davis,[1,2] Julie K. Jadlowsky,[2] Gabriela Plesa,[2] Donald L. Siegel,[2,3,4] Anne Chew,[2,4] Bruce L. Levine,[2,3,4] Shelley L. Berger,[6,7,8,9] Edmund K. Moon,[2,3,5] Steven M. Albelda,[2,3,5] and Joseph A. Fraietta[1,2,3,4,10,*]

[1]Department of Microbiology, Perelman School of Medicine, University of Pennsylvania, Philadelphia, PA 19104, USA
[2]Center for Cellular Immunotherapies, Perelman School of Medicine, University of Pennsylvania, Philadelphia, PA 19104, USA
[3]Abramson Cancer Center, Perelman School of Medicine, University of Pennsylvania, Philadelphia, PA 19104, USA
[4]Department of Pathology and Laboratory Medicine, Perelman School of Medicine, University of Pennsylvania, Philadelphia, PA 19104, USA
[5]Department of Medicine, Perelman School of Medicine, University of Pennsylvania, Philadelphia, PA 19104, USA
[6]Parker Institute for Cancer Immunotherapy, University of Pennsylvania, Philadelphia, PA 19104, USA
[7]Epigenetics Institute, Perelman School of Medicine, University of Pennsylvania, University of Pennsylvania, Philadelphia, PA 19104, USA
[8]Department of Cell and Developmental Biology, Perelman School of Medicine, University of Pennsylvania, Philadelphia, PA 19104, USA
[9]Department of Genetics, Perelman School of Medicine, University of Pennsylvania, Philadelphia, PA 19104, USA
[10]Lead contact
*Correspondence: jfrai@upenn.edu
https://doi.org/10.1016/j.xcrm.2023.101053

SUMMARY

Chimeric antigen receptor (CAR) T cells demonstrate remarkable success in treating hematological malignancies, but their effectiveness in non-hematopoietic cancers remains limited. This study proposes enhancing CAR T cell function and localization in solid tumors by modifying the epigenome governing tissue-residency adaptation and early memory differentiation. We identify that a key factor in human tissue-resident memory CAR T cell (CAR-T_{RM}) formation is activation in the presence of the pleotropic cytokine, transforming growth factor β (TGF-β), which enforces a core program of both "stemness" and sustained tissue residency by mediating chromatin remodeling and concurrent transcriptional changes. This approach leads to a practical and clinically actionable *in vitro* production method for engineering peripheral blood T cells into a large number of "stem-like" CAR-T_{RM} cells resistant to tumor-associated dysfunction, possessing an enhanced ability to accumulate *in situ* and rapidly eliminate cancer cells for more effective immunotherapy.

INTRODUCTION

The adoptive transfer of chimeric antigen receptor (CAR) T cells has demonstrated significant success in treating hematopoietic malignancies.[1–8] Given this advancement in the field of cellular immunotherapy, a growing number of trials now focus on solid tumors, which are responsible for more than three-quarters of cancer-related deaths worldwide.[9] However, to date, therapeutic successes in these indications, including results from our own clinical studies, have been modest (reviewed in Nguyen[10] and Martinez[11]). The reasons for poor efficacy are unknown but likely multifactorial. Unlike the situation in hematologic malignancies, CAR T cells must successfully localize from the blood to solid tumor sites despite potential T cell-/tumor-derived chemokine mismatches[12,13] and subsequently infiltrate cancer-derived extracellular matrix components to elicit cytotoxicity,[14] frequently in the setting of antigen heterogeneity or loss.[15] Even with adequate trafficking and infiltration, engineered T cells become rapidly hypofunctional in the tumor microenvironment (TME).[16,17] In addition to tumor-mediated immunosuppression, lack of therapeutic levels of *in vivo* CAR T cell expansion, local persistence at tumor sites, and elicitation of robust effector functions are attributed to T cell-intrinsic mechanisms that hamper intratumoral accumulation, resulting in treatment resistance and disease progression.[18,19]

Attrition of CAR T cell-intrinsic memory functions has been implicated in poor CAR T cell persistence and lack of durable tumor control.[20] Memory $CD8^+$ T cell subsets can be generally categorized into circulating stem cell memory (T_{SM}), central memory (T_{CM}), and effector memory (T_{EM}) T cells,[21] in addition to tissue-resident memory (T_{RM}) T cells, which mainly persist in non-lymphoid compartments without recirculation.[22–25] Current CAR T cell production methods incorporating circulating T cells have been heavily influenced by use in hematological malignancies where the ideal CAR T cells would traffic to secondary lymphoid organs and bone marrow. Thus, T_{SM} and T_{CM} with high levels of homing receptor expression and the ability to persist in lymphoid compartments have been favored. However, for solid tumor indications, CAR T cells need to localize within non-lymphoid tissues, persist, and maintain durable antitumor

activity. Thus, changing the phenotype of conventional circulating CAR T cells to more efficiently accumulate, persist, and maintain potency in the TME is an important goal.

Large fractions of tumor-infiltrating lymphocytes (TILs) are composed of T_{RM} cells, with the degree of T_{RM} infiltration directly correlating with effective endogenous antitumor responses as well as successful immunotherapy.[26–29] $CD8^+$ T_{RM} cells upregulate multiple adhesion molecules, including CD103 and CD49a, to enable T cell interactions with tumor cells and the surrounding extracellular matrix. In addition, T_{RM} cells decrease expression of migratory pathways governed by Krüppel-like factor 2 (KLF2), which dictate T cell commitment to recirculation.[30] These specific molecular features enable T_{RM} cells to accumulate at tumor sites and exert robust effector functions.

Transcription factors such as RUNX3 and cytokines including transforming growth factor beta (TGF-β), interleukin (IL)-7, and IL-15 regulate the differentiation, localization and function of long-lived $CD8^+$ T cells residing in healthy non-lymphoid tissues.[31–33] In recent studies, T_{RM} cells possessing characteristics of "stemness" were observed in normal peripheral tissues and tumor-draining lymph nodes of syngeneic mice.[34,35] These stem-like T_{RM} cells exhibit superior polyfunctionality as well as memory functions relative to their conventional resident T cell counterparts and can give rise to fully differentiated T_{RM} progeny cells in an antigen-dependent manner. Neoantigen-specific TILs possessing these characteristics have been implicated in mediating effective antitumor immunity in the setting of immune checkpoint blockade (ICB) therapies.[36] Thus, the differentiation trajectory of CAR T cells can be modulated through targeted chromatin remodeling and subsequent transcriptional changes, a process referred to as epigenetic reprogramming. By inducing these changes, we aim to create populations of CAR T cells that efficiently accumulate in tumors while maintaining robust effector functions and self-renewal capacity, potentially representing a promising treatment modality for certain cancers.

Here, we intended to enhance CAR T cell accumulation and function in solid tumors through modulation of T_{RM} fate specificity. In this vein, we explored different methods to endow human CAR T cells with both early memory features and the ability to establish tissue residency. We report the preclinical development of the proposed CAR-T_{RM} cell therapy evaluated in both solid and liquid cancer models, in addition to exploring the molecular signals promoting tissue residency, exhaustion, and early memory T cell differentiation.

RESULTS

TGF-β induces resident memory CAR T cell differentiation

TGF-β has been implicated in T_{RM} cell differentiation in non-lymphoid tissues.[37–39] Because CAR T cells are generally produced *in vitro* after activation through CD3 and CD28 ligation, we hypothesized that the presence of TGF-β during CAR T cell production would enhance the formation of engineered T_{RM} cells. To evaluate the impact of TGF-β on the phenotype of CAR T cells, different levels of TGF-β were treated during the manufacture of anti-mesothelin (M5) CAR T cells (Figure S1A). The expression of resident memory markers progressively increased as the concentration of TGF-β was increased and reached saturation at concentrations above 2 ng/mL (Figure S1B). However, the expansion capacity of the CAR T cells was compromised at 10 ng/mL (Figure S1C). To determine the optimal duration of TGF-β treatment, we tested different durations (Figure S1D). The addition of TGF-β after day 3 significantly reduced the development of the resident memory population (Figure S1E), and the CAR T cell expansion was consistent regardless of the duration of TGF-β exposure (Figure S1F). Based on these results, we used a concentration of 2 ng/mL TGF-β starting on day 0 in subsequent experiments. We then characterized the phenotype of M5 CAR T cells produced under these optimal culture conditions. Compared with conventional CAR T cells (CAR-T_{CONV}) cultured in IL-2 alone, CAR T cells that were also exposed to TGF-β (CAR-T_{RM}) upregulate several classical T_{RM} markers, including CD103, CD39, and CD49a (Figures 1A and 1B). In addition to these adhesion molecules, increased expression of inhibitory receptors is a hallmark of T_{RM} cells.[37,38,40,41] Consistent with this previous finding, CAR-T_{RM} cells showed elevated expression of PD1, LAG3, and TIM3 inhibitory receptors as well as the exhaustion-related transcription factor, TOX (Figure 1C). Intriguingly, unlike differentiated effector-like resident memory T cells, CAR-T_{RM} products express high levels of proteins that play a central role in maintaining stemness, such as TCF1 and IL7R and the lymph node homing receptor, CCR7, suggesting that TGF-β exposure reprograms T cells toward a stem-like resident memory fate (Figure 1D).[31,34,35]

TGF-β is known to have immunosuppressive effect on T cells.[42,43] We co-cultured M5 CAR T cells with the target pancreatic cancer cell, AsPC-1, to assess the antigen-dependent effector function of CAR-T_{RM} cells. Despite a marked increase in the expression of CD103, which is known be associated with enhanced cytolytic activity of resident memory T cells,[44] CAR-T_{RM} cell cytotoxic function is diminished (Figures 1E and 1F). However, CAR-T_{RM} cells show enhanced production of multiple effector cytokines (i.e., interferon gamma [IFN-γ], IL-2, tumor necrosis factor alpha [TNFα], IL-6), compared with CAR-T_{CONV} cells and exhibit a comparable level of *ex vivo* expansion during production, implying that proliferative capacity and certain T cell effector functions are not compromised by TGF-β (Figures 1G and 1H).

The function of CAR-T_{RM} cells was also evaluated during chronic antigen stimulation. Despite having lower cytolytic activity compared with CAR-T_{CONV} cells, CAR-T_{RM} cells showed a high production of IFN-γ, TNFα, and IL-6 and an increased proliferative capacity after repetitive CAR activation (Figures S2A–S2C). To determine the susceptibility of CAR T cells that were exposed to TGF-β during manufacturing to high levels of TGF-β present in the TME, CAR-T_{CONV}, and CAR-T_{RM} cells were co-incubated with target pancreatic cancer cells, with or without exogenous TGF-β. The results showed that both CAR-T_{CONV} and CAR-T_{RM} cells decreased in cytotoxicity and effector cytokine production when exposed to TGF-β (Figures S2D and S2E). However, CAR-T_{RM} cells maintained higher levels of effector cytokine production even after exposure to TGF-β, compared with CAR-T_{CONV} cells. This suggests

CellPress
OPEN ACCESS

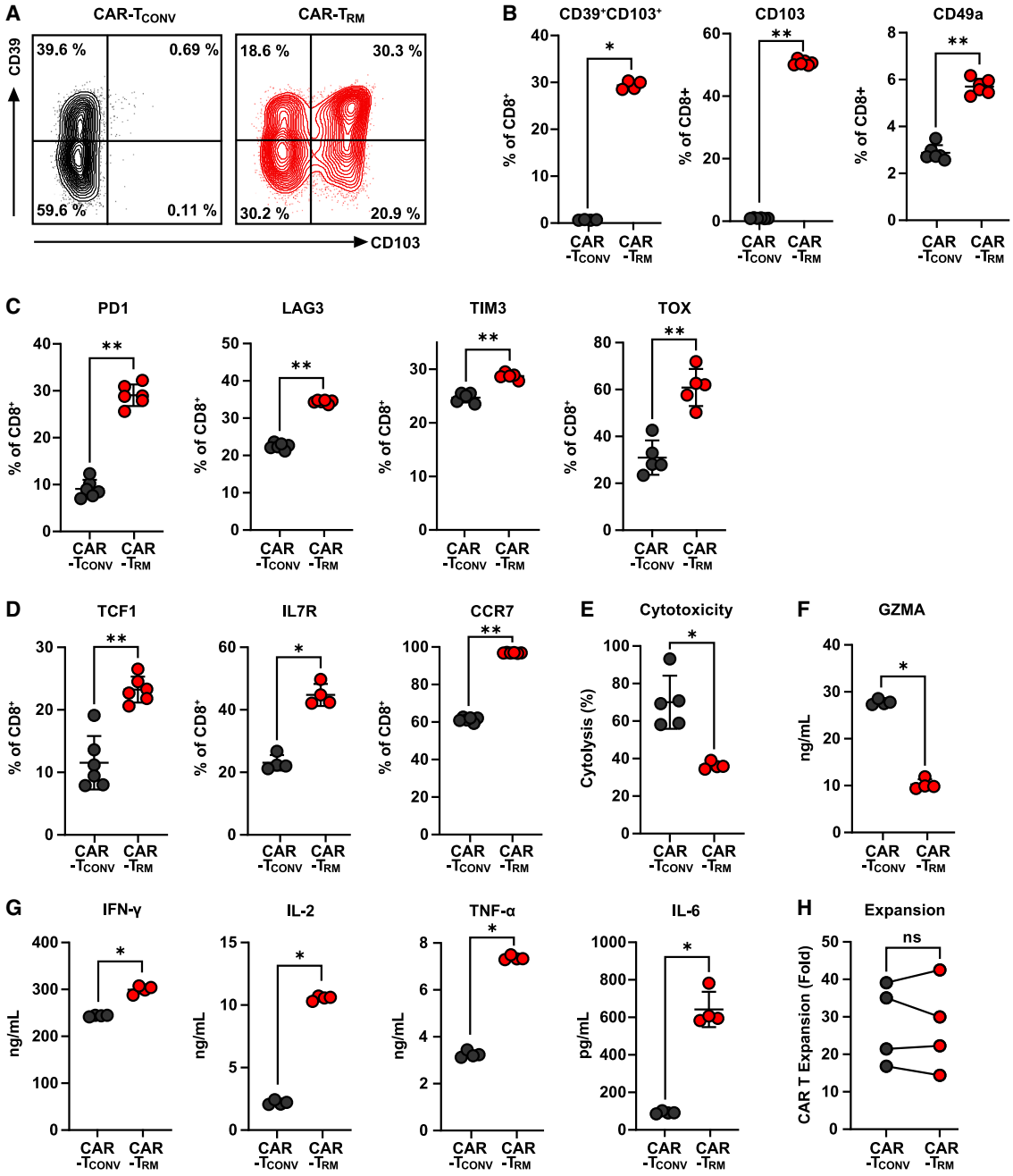

Figure 1. Phenotypic and functional characterization of CAR-T_{RM} cells

CAR T cells were cultured in T cell medium with or without 2 ng/mL TGF-β. (A) Representative flow cytometry plot showing CD39 and CD103 expression on $CD8^+$ CAR T cells after manufacturing.

(B–D) Expression markers associated with (B) residency (CD39, CD103, CD49a), (C) exhaustion (PD1, LAG3, TIM3, TOX), and (D) memory/stemness (TCF1, IL7R, CCR7) in $CD8^+$ CAR T cells.

(E) Anti-mesothelin M5 CAR T cells were co-cultured with AsPC-1 tumor targets at an effector to target (E:T) ratio of 1:2. Cytolytic activity of CAR-T_{CONV} and CAR-T_{RM} cells was measured in real time using the xCELLigence RTCA system. Cytotoxic capacity at 7 h post co-culture is shown.

(F and G) M5 CAR T cells were challenged with AsPC-1 targets at an E:T ratio of 2:1. Supernatant was collected at 18 h after coincubation, and cytokine levels were measured. (F) Granzyme A; (G) effector cytokines (IFN-γ, IL-2, TNFα, IL-6).

(H) CAR T cell expansion levels were measured during *ex vivo* manufacturing. Data represent results from four independent CAR T cell manufacturing experiments (paired t test). All *in vitro* experiments were performed using CAR T cells derived from various healthy subjects as biological replicates (n = 4–6). (A–G) Representative results from one donor. *p < 0.05; *p < 0.01; ***p < 0.001; ns, not significant (Mann-Whitney U test).

that adding TGF-β during CAR T cell manufacturing does not make the CAR T cells more susceptible to the immunosuppressive effects of TGF-β.

In recent studies, an increase in the population of regulatory CAR T cells (CAR-T_{REG}) cells has been linked to resistance to CD19 CAR T cell therapy.[45,46] To assess whether TGF-β treatment during CAR T cell manufacturing could lead to the development of CAR-T_{REG} cells, we analyzed the frequencies of $FOXP3^+CD4^+$ or $FOXP3^+IL2RA^+$ $CD4^+$ or $CD8^+$ cells between CAR-T_{CONV} cells and CAR-T_{RM} populations in multiple healthy subjects. Our results showed no significant differences, implying that transient exposure to TGF-β at the 2 ng/mL concentration used to program residency may not be sufficient to induce CAR-T_{REG} cells (Figure S2F), which is concordant with the findings of a previous study.[47]

CAR-T_{RM} cells exhibit a resident memory transcriptional program

Flow cytometric analysis of CAR-T_{RM} cells reveals acquisition of a resident memory phenotype through TGF-β signaling. To expand this finding, we sought to obtain a comprehensive view of the transcriptional landscape of CAR-T_{RM} cells by performing bulk RNA sequencing (RNA-seq). Principal-component analysis of transcriptome data indicated that TGF-β exposure was the strongest driver of transcriptional variance across multiple donors (Figure 2A). Consistent with our flow cytometry data, CAR-T_{RM} cells are significantly enriched in $CD69^+CD103^+CD8^+$ resident memory T cell gene signatures and exhibit reduced $CD69^-CD103^-CD8^+$ non-resident memory T cell transcriptional profiles (Figure 2B). Specifically, CAR-T_{RM} express high levels of resident memory-associated genes encoding cell surface molecules (*ITGAE*, *PDCD1*) and transcription factor genes (*BHLHE40*, *EGR2*, *NR4As*, *IRF4*) while downregulating *KLF2*, which is essential for T cell recirculation and inhibition of T_{RM} cell differentiation (Figures 2C and 2D).[30] This increased resident memory transcriptional program in CAR-T_{RM} cells may be partially attributed to hypoxia pathway upregulation, which is known to facilitate resident memory T cell differentiation, indicating a possible overlap between TGF-β signaling and responses to low oxygen tension (Figures 2E and S3).[44,48]

One of the major barriers that limits the antitumor potency of cell therapies derived from circulating lymphocytes is poor trafficking and infiltration to tumors surrounded by an extracellular matrix (ECM). CAR-T_{RM} cells upregulate genes encoding integrins, laminin, type I heparan sulfate proteoglycan, and matrix metalloproteinases (MMPs), which degrade various ECM proteins and enriched pathways related to ECM regulation and cell migration (Figures 2F and 2G; Table S1). Accordingly, tumor-infiltrating T cells (TILs) that clonally expand in response to ICB therapy exhibit a tissue-resident memory transcriptional program in responding oral cancer patients.[49] We thus sought to examined whether TGF-β-generated CAR-T_{RM} cells share transcriptional features of these favorable resident memory subsets observed in ICB responders. Gene set enrichment analysis indicates that CAR-T_{RM} cells significantly upregulate signatures enriched in pre- and post-treatment TILs that expand upon response to anti-programmed cell death protein 1 (PD-1)/cytotoxic T lymphocyte–associated protein 4 (CTLA-4) treatment, while downregulating gene sets found in tumor-infiltrating T cells that fail to respond to ICB (Figure 2H). Altogether, our bulk RNA-seq analyses suggest that CAR-T_{RM} cells acquire a favorable and clinically relevant transcriptional program of tissue residency.

CAR-T_{RM} cells show transcriptional features of stem-like resident memory T cells

Our bulk analyses indicate that CAR-T_{RM} cells elevate markers of both tissue residency and T cell stemness (Figures 1B and 1D). We further explored how these residency- and stemness-related transcriptional programs are regulated in CAR-T_{RM} cells using single-cell RNA-seq (scRNA-seq). CAR-T_{CONV} and CAR-T_{RM} were harvested after 9 days of expansion and processed for scRNA-seq. After removal of low-quality cells, 12,230 cells were obtained. Uniform Manifold Approximation and Projection (UMAP) clustering of $CD8^+$ T cells reveal three clusters with discrete transcriptional features (Figure 3A). Notably, a $TCF7^+CD8^+$ CAR-T_{RM} subset expresses high levels of stemness-related genes such as *TCF7* and *IL7R* (Figures 3B, S4A, and S4B). Consistent with this gene expression profile, $TCF7^+CD8^+$ CAR-T_{RM} cells are enriched in a core transcriptional program of stem-like $CD8^+$ T cells possessing self-renewal potential (Figure S4C). In addition, $MKI67^+CD8^+$ CAR-T_{RM} cells upregulate G2M and S phase pathways as well as other cell cycle-related genes (*MKI67*, *CDCA8*, *CDCA6*, *CDKN3*, *CDK1*, *CDC25B*) while downregulating memory-related genes and signatures associated with successive linear T cell differentiation (Figures 3A, 3B, and S4A–S4C). These findings are consistent with the proposed model and support the idea that $MKI67^+CD8^+$ CAR T cells predominantly represent the replicating fraction. $CD27^+CD8^+$ CAR-T_{RM} cells exhibit intermittent transcriptional features between those of $TCF7^+CD8^+$ and $MKI67^+CD8^+$ populations, as manifested by elevated expression of central memory T cell genes (*CD27*, *SELL*), along with T cell activation and cytotoxic effector genes (*HLA-B*, *GZMA*, *HLA-B*, *HLA-A*, *CD69*) (Figure 3B). In accordance with a previous report of TGF-β preserving $TCF1^+$ precursor cells in chronic infection,[50] CAR-T_{RM} cells are enriched in stem-like $TCF7^+CD8^+$ T cells with concordant gene signatures and composed of reduced frequencies of more differentiated subsets (e.g., $CD27^+CD8^+$ and $MKI67^+CD8^+$) compared with the CAR-T_{CONV} counterpart (Figures 3A and S4C).

As observed in bulk RNA-seq analysis, CAR-T_{RM} cells increase expression of resident memory T cell genes and related signatures and reduce *KLF2* and $CD69^-CD103^-CD8^+$ gene set expression (Figures 3C and 3D; Table S2). A series of recent studies demonstrated that stem-like progenitor and resident memory cells that persist in tumors give rise to the proliferative burst of neoantigen-specific T cells and drive antitumor activity in response to ICB blockade.[27,36,49,51,52] These reports suggest that stemness and resident memory programs could be optimal transcriptional features for cellular immunotherapies. Thus, we asked whether the resident memory transcriptional program is preserved in the stem-like CAR-T_{RM} cells by conducting gene expression and pathway analysis in the $TCF7^+CD8^+$ cluster. Similar to what we observed in bulk $CD8^+$ populations, CAR-T_{RM} increased resident memory-associated genes

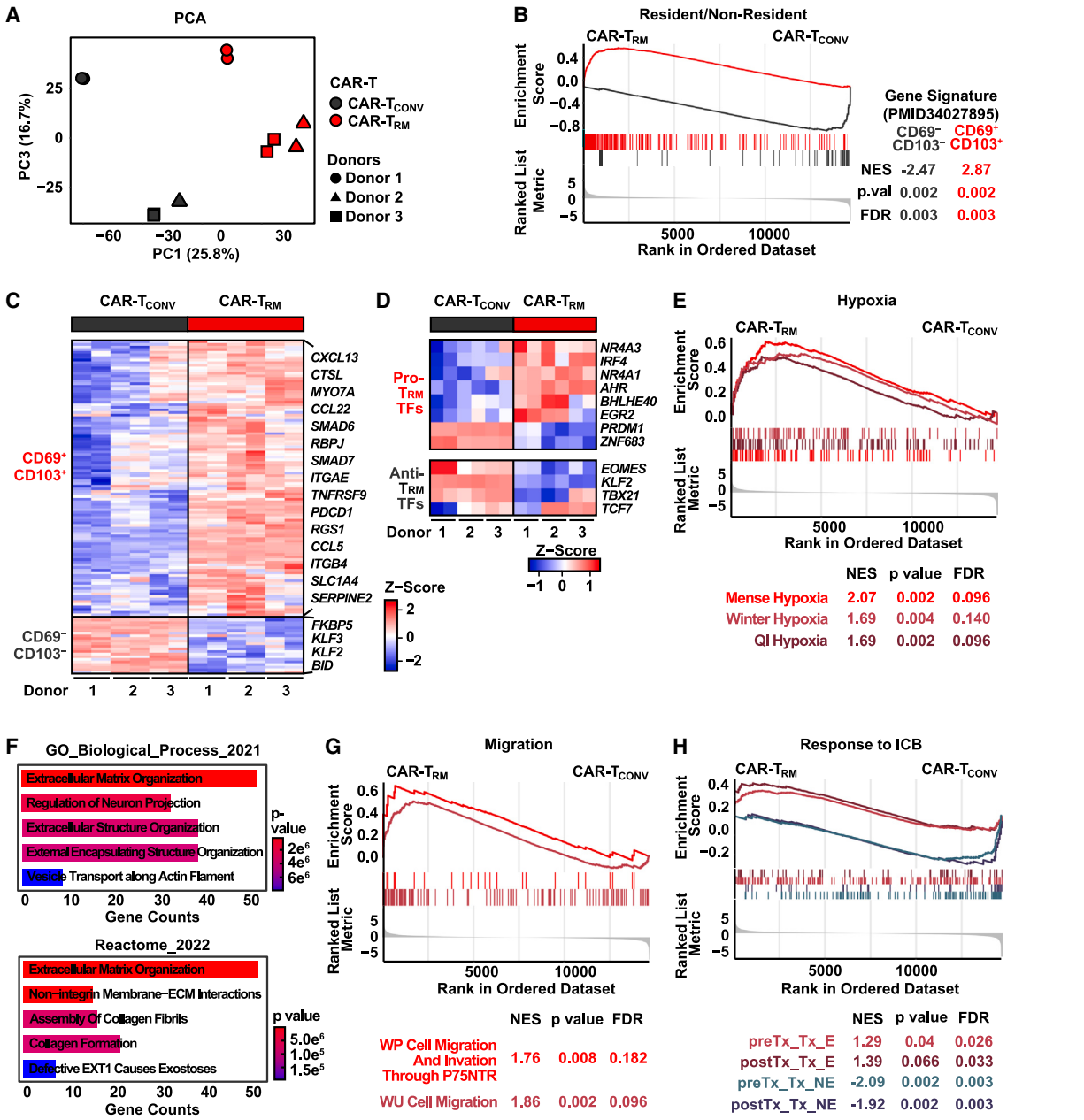

Figure 2. CAR-T_{RM} cells possess a core resident memory transcriptomic signature

Bulk RNA-seq experiments were conducted using $CD8^+$ CAR-T_{CONV} and CAR-T_{RM} cells.

(A) Principal-component analysis was carried out with RNA expression data.

(B) Gene set enrichment analysis (GSEA) using gene sets associated with resident memory T cells.

(C) Heatmap showing differentially expressed genes from $CD69^+CD103^+$ and $CD69^-CD103^-CD8^+$ T cell signatures.

(D) Heatmap displaying expression of transcription factor genes known to promote and suppress resident memory T cell differentiation.

(E) GSEA (hypoxia pathways: MSigDB C2).

(F) Pathway analysis incorporating genes upregulated in CAR-T_{RM}-cells using Enrichr.

(G) GSEA analysis (migration pathways: MSigDB C2). GSEA with gene signatures of tumor-infiltrating T cells associated with response to ICB. Bulk RNA-seq experiments were conducted using CAR T cells derived from n = 3 distinct healthy donors, serving as biological replicates.

(e.g., *ITGAE*, *BHLHE40*, *CCL5*) and T_{RM} transcriptional signatures as well as early memory genes (*IL7R*, *STAT3*), whereas it downregulated genes associated with circulation (e.g., *KLF2*) and non-resident memory signatures (Figures 3E–3G; Table S2). These data suggest that TGF-β-produced CAR-T_{RM} cells harbor a pool of stem-like cells, which could potentially persist and give rise to large numbers of differentiated resident memory progeny cells in tumors.[34,35]

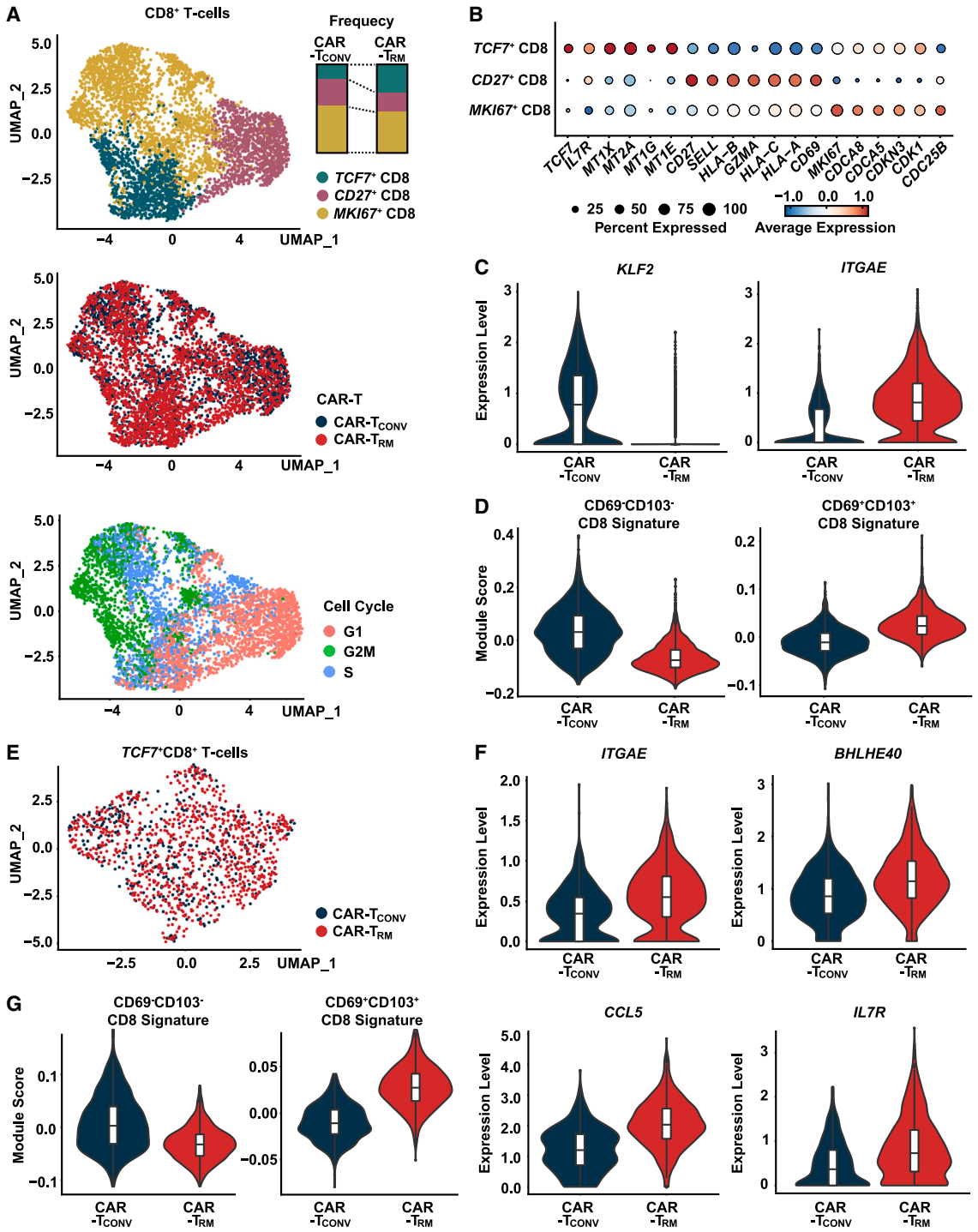

Figure 3. TGF-β-generated CAR-T_{RM} cells transcriptionally resemble stem-like T_{RM} cells

(A) UMAP imbedding of $CD8^+$CAR T cell (top, CD8 subclusters; middle, CAR T cell samples; bottom, cell cycle). Frequencies of three $CD8^+$ clusters in CAR-T_{CONV} and CAR-T_{RM} cells are shown.

(B) Bubble plot displaying expression levels of marker genes in each $CD8^+$ subcluster.

(C) Violin plots showing expression of *KLF2* and *ITGAE*.

(legend continued on next page)

Epigenetic reprogramming of stem-like CAR-T_{RM} cells sustains a persistent resident memory phenotype during chronic antigen stimulation

Epigenetic modification leads to durable changes in gene expression, sets thresholds for future gene transcription, and plays an important role stabilizing T cell differentiation fate.[53–56] In this regard, we investigated whether transient exposure to TGF-β during CAR T cell production can induce epigenetic rewiring of CAR-T_{RM} cells to sustain the acquired stem-like resident memory phenotype. We thus conducted assay for transposase-accessible chromatin with sequencing (ATAC-seq) to assess the global chromatin accessibility of CAR-T_{CONV} and CAR-T_{RM} cells. As seen in our transcriptional studies, CAR-T_{RM} differentiation mediates the largest epigenetic variance across donors and induces global chromatin remodeling (Figures 4A and 4B). Gene set enrichment analysis with differentially accessible regions suggests that CAR-T_{RM} cells are enriched in a $CD69^+CD103^+CD8^+$ signature while downregulating a $CD69^-CD103^-CD8^+$ chromatin landscape profile (Figures 4C and 4D). Consistent with these observations, chromatin accessibility is significantly increased at resident memory gene loci (e.g., *ITGAE*, *ITGAV*, *ENTPD1*, *IRF4*) and decreased at non-resident memory genes (e.g., *KLF2*) in CAR-T_{RM} cells (Figures 4E and 4F). Additionally, peaks were enriched in stemness-related gene regions such as *TCF7* and *IL7R* in CAR-T_{RM} cells (Figure 4G). Based on these findings, we then asked whether this epigenetic rewiring of stem-like CAR-T_{RM} cells can sustain a resident memory phenotype during chronic antigen stimulation. We therefore repetitively challenged mesothelin-directed CAR-T_{RM} cells with irradiated AsPC-1 tumor targets without additional supplementation of exogenous TGF-β and assessed their resident memory phenotype over time. Notably, TGF-β-generated CAR-T_{RM} cells maintain both tissue-resident ($CD103^+CD39^+CD8^+$ and $CD103^+CD49a^+CD8^+$) and stem-like resident memory ($CD103^+IL7R^+CD8^+$) phenotypes following repetitive tumor challenge, suggesting that epigenetic reprogramming may contribute to the stability of these differentiation fates (Figures 4H and S5).

CAR-T_{RM} cells exhibit transcriptional and epigenetic features of exhaustion but show enhanced effector function

One of the major barriers to efficacious CAR T cell therapy is T cell exhaustion, which is characterized by sustained expression of multiple inhibitory checkpoint receptors, reduced proliferative capacity, and diminished antitumor effector functions.[57–59] T_{RM} cells are known to exhibit certain transcriptional features of T cell exhaustion, such as upregulation of inhibitory receptor encoding genes.[44,60] Given that CAR-T_{RM} cells show increased expression of PD1, LAG3, TIM3, as well as the exhaustion-related transcription factor, TOX (Figure 1C), we sought to further investigate the transcriptional and epigenetic properties of exhaustion in CAR-T_{RM} cells. We first conducted motif analysis to identify transcription factors involved in CAR-T_{RM} cell differentiation and found that basic leucine zipper (bZIP) and interferon regulatory factor (IRF) binding sites were the most significantly enriched in CAR-T_{RM} cells, which is an epigenetic hallmark of exhausted CAR T cells (Figure 5A).[61] Consistent with these findings, transcriptional analysis reveals that several bZIP and IRF transcription factor genes (*ATF3*, *IRF4*, *ATF4*, *BATF3*, *ATF2*, *ATF6*) were highly elevated in CAR-T_{RM} cells, while canonical AP-1 transcription factors (*JUN*, *FOS*), which are required for optimal T cell expansion and effector function, were downregulated (Figure 5B). Transcriptional signatures associated with human T cell exhaustion were also enriched in CAR-T_{RM} cells (Figure 5C). We investigated whether the enrichment of exhaustion signatures is specific to a particular subpopulation of $CD8^+$ CAR-T_{RM} cells. We compared the exhaustion signature scores of CAR-T_{CONV} and CAR-T_{RM} cells within each $CD8^+$ CAR T cell subset identified in scRNA-seq. Our results showed that, in all three CD8 subsets, CAR-T_{RM} cells displayed an upregulation of exhaustion pathways compared with CAR-T_{CONV} cells. This suggests that the programming of T_{RM} cells regulates exhaustion independently of the cell state (Figures S6A and S6B). Altogether, these results indicate that despite sustained antigen-specific proliferation and enhancement of effector cytokine production (Figures 1G and 1H), CAR-T_{RM} cells exhibit several epigenetic and transcriptional signs of exhaustion (Figures 5B and 5C). The enhanced effector cytokine production capability of CAR-T_{RM} cells can be partly attributed to the distinctive transcriptional and epigenetic characteristics that set CAR-T_{RM} cells apart from terminally exhausted T cells. Notably, CAR-T_{RM} cells exhibit decreased expression of *PRDM1* (logFC = −1.26, $p < 0.001$), *ID2* (logFC = −0.34, $p = 0.007$), and *TOX2* (logFC = −0.73, $p = 0.002$), and increased transcript levels of *ID3* (logFC = 0.61, $p = 0.007$) (Table S1). *PRDM1*, *ID2*, and *TOX2* are known to promote terminal differentiation, T cell exhaustion, CAR T cell dysfunction, and loss of stemness and polyfunctionality,[19,62–66] while *ID3* has been shown to preserve stemness, enhance IL-2 and TNFα production, and prevent terminal exhaustion.[34,67] Correspondingly, CAR-T_{RM} cells demonstrate reduced chromatin accessibility at *PRDM1*, *ID2*, and *TOX2* gene regions (Figure S6C).

Resident memory and exhaustion-related transcriptomic programs share several transcription factors, such as *IRF4*, *NR4A* family genes, and *EGR2* (Figure 5B).[38,68–70] To gain a deeper understanding of the role of these transcription factors on the regulation of T cell residency and exhaustion programs, we deleted these transcription factor genes in CAR-T_{CONV} and CAR-T_{RM} cells and assessed the immunophenotype of these knockout variants. Interestingly, *IRF4* deletion significantly decreased the number of $PD1^+TOX^+CD8^+$ T cells (Figure 5D). Furthermore, *IRF4* knockout resulted in higher production of effector cytokines (IL-2, IFN-γ) and cytotoxic molecules (perforin, granzyme A) in CAR-T_{RM} cells, enhancing their cytolytic

(D) $CD69^-CD103^-$ and $CD69^+CD103^+CD8^+$ T cell signature scores calculated for CAR-T_{CONV} and CAR-T_{RM} cells.
(E) A UMAP plot showing CAR T cell sample origin in $TCF7^+CD8^+$T cells.
(F) Expression of resident memory (*ITGAE*, *BHLHE40*, *CCL5*) and early memory (*IL7R*) markers in $TCF7^+CD8^+$ T cells.
(G) Module score comparison for $CD69^-CD103^-$ and $CD69^+CD103^+$ $CD8^+$ T cell signatures between CAR-T_{CONV} and CAR-T_{RM} $TCF7^+CD8^+$ T cells.

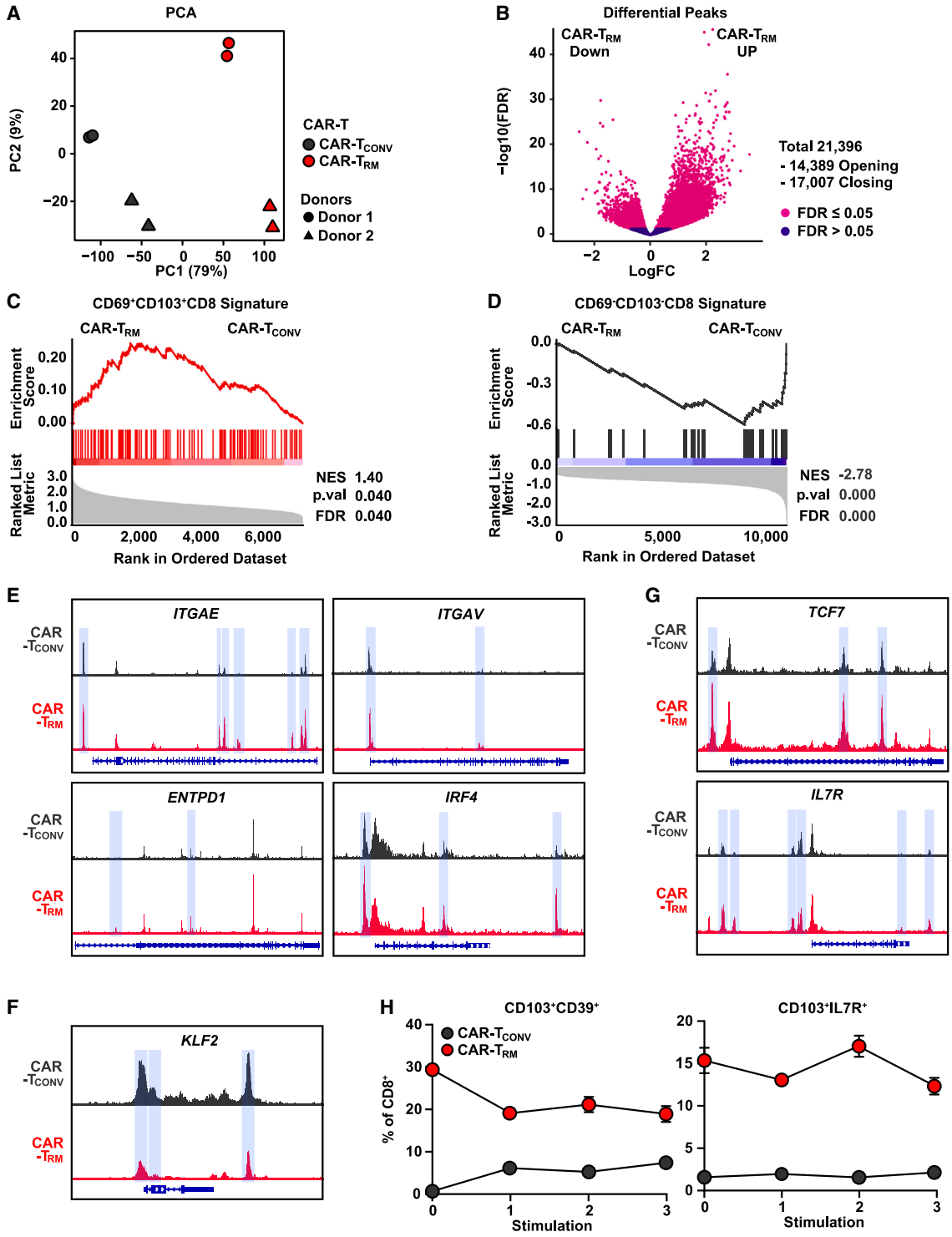

Figure 4. Chronically stimulated stem-like CAR-T_{RM} cells sustain a resident memory phenotype in association with epigenetic reprogramming

(A) Principal-component analysis of ATAC-seq data.

(B) Volcano plot demonstrating differentially accessible peaks between CAR-T_{RM} and CAR-T_{CONV} $CD8^+$ cells.

(C–G) GSEA showing enrichment of (C) $CD69^+CD103^+CD8^+$ and (D) $CD69^-CD103^-CD8^+$ T cell signatures. ATAC-seq tracks of genes associated with (E) resident memory T cells (*ITGAE*, *ITGAV*, *ENTPD1*, *IRF4*), (F) circulating T cells (*KLF2*), and (G) stemness (*TCF7*, *IL7R*). Differentially accessible regions are highlighted in blue.

(legend continued on next page)

capability, although *IRF4*-deficient CAR T cells showed a decreased capacity to proliferate (Figures 5E–5G and S6D). Moreover, *IRF4* knockout CAR-T_{RM} cells maintained a resident memory phenotype, showing a comparable level of CD103 expression and increased expression of CD49a compared with the *AAVS1*-deleted CAR-T_{RM} control (Figure 5H). Collectively, these studies demonstrate that *IRF4* promotes T cell exhaustion and is dispensable for induction of the resident memory phenotype in CAR-T_{RM} cells.

Stem-like CAR-T_{RM} cells demonstrate superior antitumor potency against solid and liquid tumors

We next examined the *in vivo* antitumor activity of CAR-T_{RM} cells in both solid and blood cancer models. M5 anti-mesothelin CAR-T_{RM} cells exhibit remarkable tumor control compared with CAR-T_{CONV} cells, as demonstrated in both a mesothelin-expressing xenogeneic AsPC-1 pancreatic tumor model (Figure 6A) and in the suppression of mesothelin-expressing Capan-2 pancreatic ductal adenocarcinoma (Figure 6B). To understand the phenotype of intratumoral CAR T cells, we harvested tumors on day 13 post CAR T cell injection, when the tumor size was similar among experimental groups (~600 mm^3). We found that the improved antitumor activity was due to a significant increase in the number of CAR-T_{RM} cells within the tumors (Figure 6C). This increase was partially due to improved early localization of the T cells in the tumor, as a higher number of CAR-T_{RM} cells were observed as early as 2 days after CAR T cell infusion (Figure S7A). Both CAR-T_{CONV} and CAR-T_{RM} cells are highly enriched with $CD103^+CD39^+CD8^+$ TILs, suggesting that CAR T cells with a resident memory phenotype preferentially accumulate at tumor sites (Figure 6D). Notably, mice treated with CAR-T_{RM} cells show a significant increase in the absolute number of tumor-infiltrating $CD103^+CD39^+CD8^+$ cells (Figure 6D), which indicates that the TGF-β-induced stem-like resident memory population can give rise to a large number of resident memory CAR-TILs. Consistent with our *in vitro* results, CAR-T_{RM} cells in the tumor show upregulated expression of IL7R and other early memory markers (Figures 6E and S7B). Additionally, CAR-T_{RM} cells increased frequencies of T cells co-expressing multiple inhibitory receptors (Figure 6F). Despite this exhaustion-like phenotype, CAR-T_{RM} cells harvested from pancreatic tumors demonstrate enhanced TNFα, perforin, and granzyme B production compared with CAR-T_{CONV} products, further underscoring that the exhaustion-like phenotype and CAR T cell antitumor effector function are decoupled (Figures 6G and S7C). Given the high expression of memory markers in CAR-T_{RM} cells, we investigated their ability to provide durable antitumor activity against a secondary tumor challenge. Mice that had previously rejected Capan-2 tumors and received CAR-T_{RM} cell treatment were re-challenged with Capan-2 cells, while a control group of CAR-T_{RM}-naive mice was also given Capan-2 cells (Figure 6H, left). Notably, the CAR-T_{RM} cells successfully prevented tumor growth, while the control group did not (Figure 6H, right). These results suggest that CAR-T_{RM} cells confer long-lasting protection against tumors. Next, to investigate the contribution of the resident memory cell population to the degree of antitumor activity, we depleted the $CD103^+$ population in CAR-T_{RM} cell products and assessed their potency *in vivo* (Figure 6I). The removal of $CD103^+$ T cells partially impairs tumor control mediated by CAR-T_{RM} cells, suggesting that this subset is required for optimal efficacy (Figure 6J). We also tested CAR-T_{RM} cells in an aggressive B cell leukemia xenograft model. Anti-CD19 CAR-T_{RM} cells prevent tumor growth and markedly improve mouse survival (Figures 6K and 6L). Analysis of peripheral blood revealed that CAR-T_{RM} cells increase *in vivo* CAR T cell expansion capacity due to enhanced early memory differentiation (Figures 6M and 6N).

Building on the findings from previously examined solid and blood cancer models, we evaluated the *in vivo* antitumor activity of CAR-T_{RM} cells in an intraosseous prostate tumor model, using PC3 prostate tumor cells engineered to express PSMA (PC3-PSMA). A single infusion of PSMA CAR-T_{RM} cells led to a significant reduction in bioluminescent tumor burden compared with CAR-T_{CONV} cells in mice bearing intraosseous tumors generated by PC3-PSMA cell engraftment (Figure S7D). Moreover, CAR-T_{RM} cells not only effectively controlled tumor growth but also resulted in prolonged survival for the mice compared with CAR-T_{CONV} cells (Figure S7E), further highlighting the potential therapeutic advantages of CAR-T_{RM} cells.

RUNX3 is a key transcription factor essential for the establishment of tissue-resident T cells, and ectopic overexpression of this transcription factor enhances $CD103^+CD8^+$ T cell differentiation in murine models.[31] We therefore compared forced expression of RUNX3 with TGF β treatment in the context of generating optimally potent CAR-T_{RM} cells. To compare these engineering strategies, we employed an *in vivo* CAR T cell stress test based on the use of a tonically signaling anti-mesothelin CAR construct (SS1)[71] and our previously characterized, highly treatment-resistant mesothelioma model incorporating a human mesothelioma cell line transduced to express mesothelin (EMMESO cells).[72] Clinically, this CAR construct demonstrates limited clinical efficacy against malignant pleural mesothelioma, pancreatic ductal adenocarcinoma, and ovarian cancer due to poor persistence and a low level of tumor infiltration.[73] Human RUNX3 was successfully overexpressed in SS1 CAR T cells through lentiviral transduction (Figure 7A). Notably, unlike TGF-β-generated CAR-T_{RM} products enriched with resident memory $CD8^+$ T cells, RUNX3 overexpression was unable to induce expression of tissue-resident markers such as CD103, CD39, and CD49a despite an increase in T cell activation as indicated by CD25 expression (Figure 7B). We next assessed the *in vivo* antitumor potency of these differentially engineered CAR T cells in mice engrafted with EMMESO cells. While TGF-β-reprogrammed CAR-T_{RM} cells successfully enhance tumor control, CAR T cells overexpressing RUNX3 fail to suppress tumor growth (Figure 7C).

(H) M5 CAR T cells were repetitively challenged with AsPC1 cells, and frequencies of resident memory ($CD103^+CD39^+CD8^+$) and stem-like resident memory ($CD103^+IL7R^+CD8^+$) T cells are shown over time. Bulk ATAC-seq experiments were performed using manufactured $CD8^+$ CAR T cells from n = 2 healthy donors as biological replicates. Restimulation assays were performed with CAR T cells generated from n = 3 distinct healthy subjects, also serving as biological replicates. Results from one representative donor are shown.

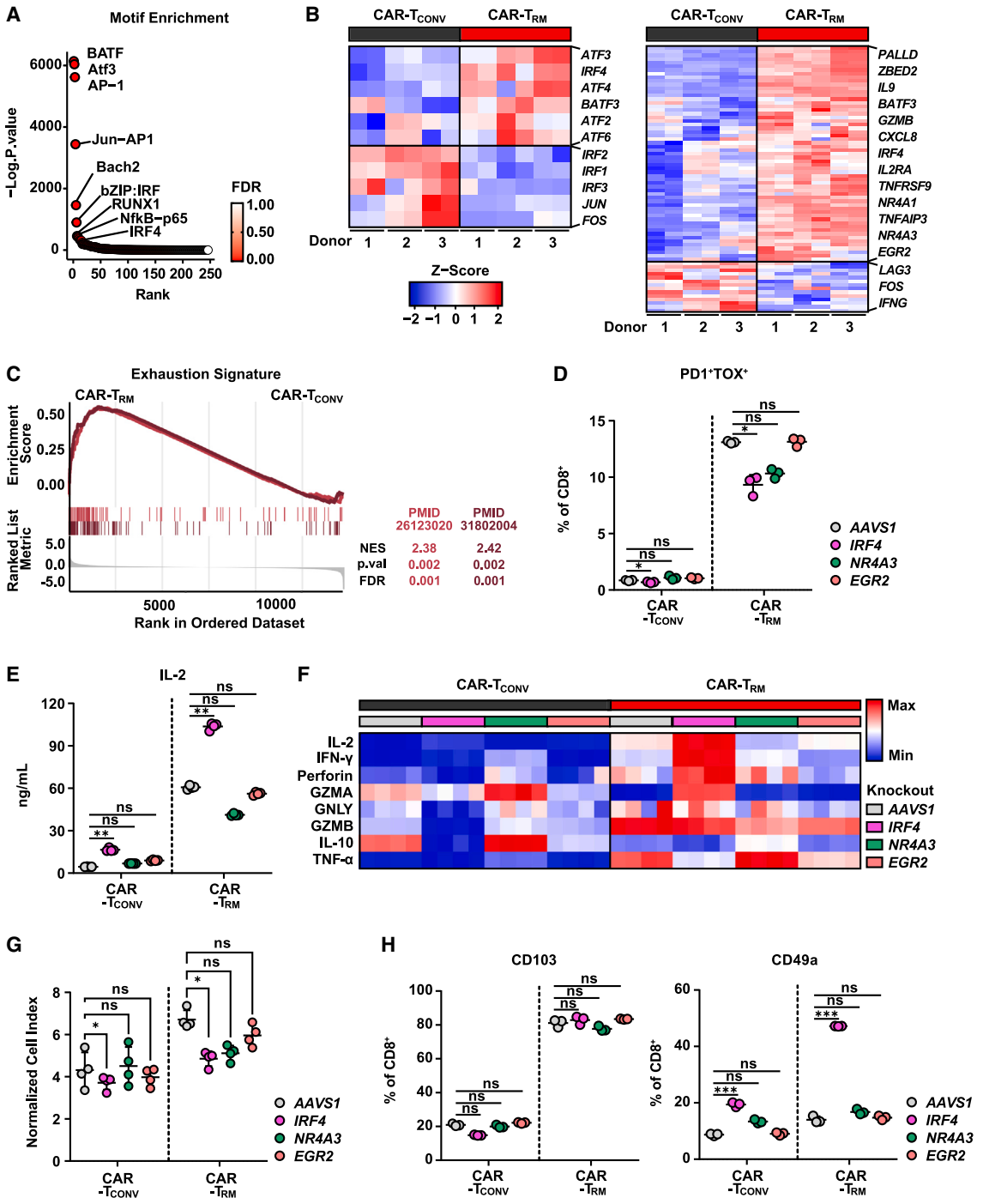

Figure 5. Highly functional CAR-T_{RM} cells appear to be transcriptionally and epigenetically exhausted

(A) Top transcription factor motifs enriched in CAR-T_{RM} cells.

(B) Heatmap showing expression of bZIP and IRF transcription factor genes (left) and genes associated with CAR T cell exhaustion in $CD8^+$CAR T cells (right).

(C) GSEA showing enrichment of exhaustion signatures.

(D) The frequency of exhausted CAR T cells ($PD1^+TOX^+$ $CD8^+$) is shown (two-way ANOVA, n = 3 biological replicates).

(E and F) M5 CAR T cells were challenged with AsPC-1 tumor cells at an E:T ratio of 2:1. Supernatants were collected at 18 h after coincubation and cytokine levels measured. (E) IL-2 production levels (two-way ANOVA, n = 4 biological replicates). (F) Heatmap showing effector cytokine and cytotoxic molecule production levels.

(legend continued on next page)

DISCUSSION

In this study, we demonstrate that epigenetic rewiring of human peripheral blood T cells can produce stem-like T_{RM} CAR T cells with improved ability to accumulate in solid tumors and resist dysfunction. We explored different methods to endow CAR T cells with both early memory features and the ability to establish tissue residency. Although TGF-β is traditionally thought of as an inhibitor of T cell function,[74] we found that human T cell exposure to TGF-β during the *ex vivo* engineering process alters the epigenetic landscape of CAR T cells to a stem-like fate, which enables CAR-T_{RM} products to sustain a resident memory phenotype during experimental stress tests involving chronic antigen challenge. Furthermore, we found that although CAR-T_{RM} cells exhibit epigenetic and transcriptional characteristics commonly associated with exhaustion, these T cells were highly resistant to tumor-imposed dysfunction. Through evaluation of CAR-T_{RM} cells in both solid and liquid cancer models, we show that these products exhibit superior antitumor potency over conventional CAR T cells, as manifested by enhanced accumulation at tumor sites and elicitation of robust effector functions.

Current CAR T cell production methods rely on peripheral-blood-derived lymphocytes as the starting point for manufacturing. In the treatment of hematological malignancies, protocols that lead to enrichment of T_{SM} and T_{CM} cells with high levels of CCR7 and CD62L expression for persistence within secondary lymphoid organs and bone marrow are desired. In contrast, for solid tumors, CAR T cells need to acquire the capacity to localize and expand within non-lymphoid tissues to exert sustained antitumor activity. T_{RM} cells that naturally reside in healthy non-hematopoietic tissues and tumors may represent a promising CAR-engineered cell population for adoptive transfer to treat these latter indications. However, T_{RM}-based cell therapy approaches have been limited to date due to the technical challenges associated with the isolation and expansion of T_{RM} cells.

We sought to reprogram readily abundant circulating T cells to CAR-T_{RM} cells using a simple and actionable manufacturing process. Accordingly, we show that the presence of TGF-β during CAR T cell production promotes the robust expansion of a T_{RM}-like population. This strategy for generating CAR-T_{RM} cells induces CD103 upregulation and promotes $CD103^+$ CD8 T_{RM} cell differentiation, which is important for the long-term retention of T cells in tissues.[37,38,75] The observed partial attenuation of tumor control following depletion of $CD103^+$ T cells from adoptively transferred products supports the conclusion that acquisition of a residency phenotype is a critical element of increased CAR-T_{RM} cell potency.

We found that CAR-T_{RM} cells are enriched in a core T_{RM} transcriptomic signature composed of a transcription factor gene expression profile, including *BHLHE40*, NR4A family genes, *AHR*, *IRF4*, and *EGR2*,[44,76–78] with a concomitant downregulation of *EOMES*[79] and *KLF2*,[30] which normally function to counter T cell residency programs and promote egress from tissues/recirculation. Additional molecules whose upregulation is associated with tissue retention, such as CD39 and CD49a, are also highly expressed by TGF-β-generated CAR-T_{RM} cells, independently of other environmental cues, such as low oxygen tension.[48] These findings suggest that TGF-β alone is sufficient to induce transcriptional and functional attributes of tissue residency in the setting of CAR-engineered T cells.

Although it was previously reported that RUNX3 programs murine $CD8^+$ T_{RM} cell differentiation,[31] forced expression of RUNX3 in human CAR-T_{RM} cells was not sufficient to promote formation or enhance *in vivo* antitumor efficacy. Recently, it was reported that RUNX3 promotes a $CD8^+$ T cell tissue-residency program in a TGF-β-signaling-dependent manner.[80] Thus, additional work is needed to determine if the combination of RUNX3 overexpression and TGF-β signaling increases the potency of CAR-T_{RM} cells. There are appreciable similarities and critical differences between the phenotypes and functional attributes of mouse and human T_{RM} cells,[41,81–83] which highlights the need to investigate human T_{RM} cell differentiation further to understand the molecular underpinnings of fate programs and enable effective translational application. Thus, these findings contribute to the advancement of the use of tissue-resident T cells in cancer therapy.

An interesting aspect of this study is that human CAR T cells activated and expanded in the presence of TGF-β are epigenetically reprogramed toward a stem-like memory state, manifested at least in part by increased expression of the stemness transcription factor TCF1 (encoded by *TCF7*) in association with chromatin accessibility at the *TCF7* locus. TGF-β-generated stem-like CAR-T_{RM} cells display an epigenetic program composed of tissue-residency signatures. Although this epigenetically rewired stem-like program allowed CAR-T_{RM} cells to maintain a T_{RM} phenotype during chronic antigen stimulation, additional investigations are needed to better determine whether these imprints are fixed or amenable to epigenetic remodeling following CAR-T_{RM} cell trafficking to specific tumor tissues.

Exhaustion-related transcriptional programs are often shared between T_{RM} cells and dysfunctional T cells.[44] We demonstrate that human CAR-T_{RM} cells not only upregulate surface inhibitory receptors but also share high correlation among their chromatin profiles with those of dysfunctional CAR T cells, including increased accessibility of bZIP and IRF motifs and overexpression exhaustion-related transcription factor genes. In reference to our findings, as shown in Figure 5, the bZIP and IRF transcription factor genes (*ATF3*, *IRF4*, *ATF4*, *BATF3*, *ATF2*, *ATF6*) were found to be highly elevated in CAR-T_{RM} cells, while the canonical AP-1 transcription factor genes (*JUN*, *FOS*) were downregulated. However, as a recent study reported, the enrichment of AP-1, bZIP, and IRF motifs and upregulation of *BATF*, *JUNB*, and *IRF8* in CAR T cells was associated with enhanced tumor

(G) Cytolytic activity of M5 CAR T cells was determined by coculturing the cells with Capan-2 cells at an effector to target ratio of 1:6 after three antigen stimulations. The normalized cell index at 31 h post co-culture was measured using the xCELLigence RTCA system. Results are shown as mean ± SEM of replicates (two-way ANOVA).

(H) Frequencies of resident memory CAR T cells ($CD103^+$ or $CD49a^+$ $CD8^+$) are shown (two-way ANOVA, n = 3 biological replicates). *$p < 0.05$; *$p < 0.01$; ***$p < 0.001$; ns., not significant.

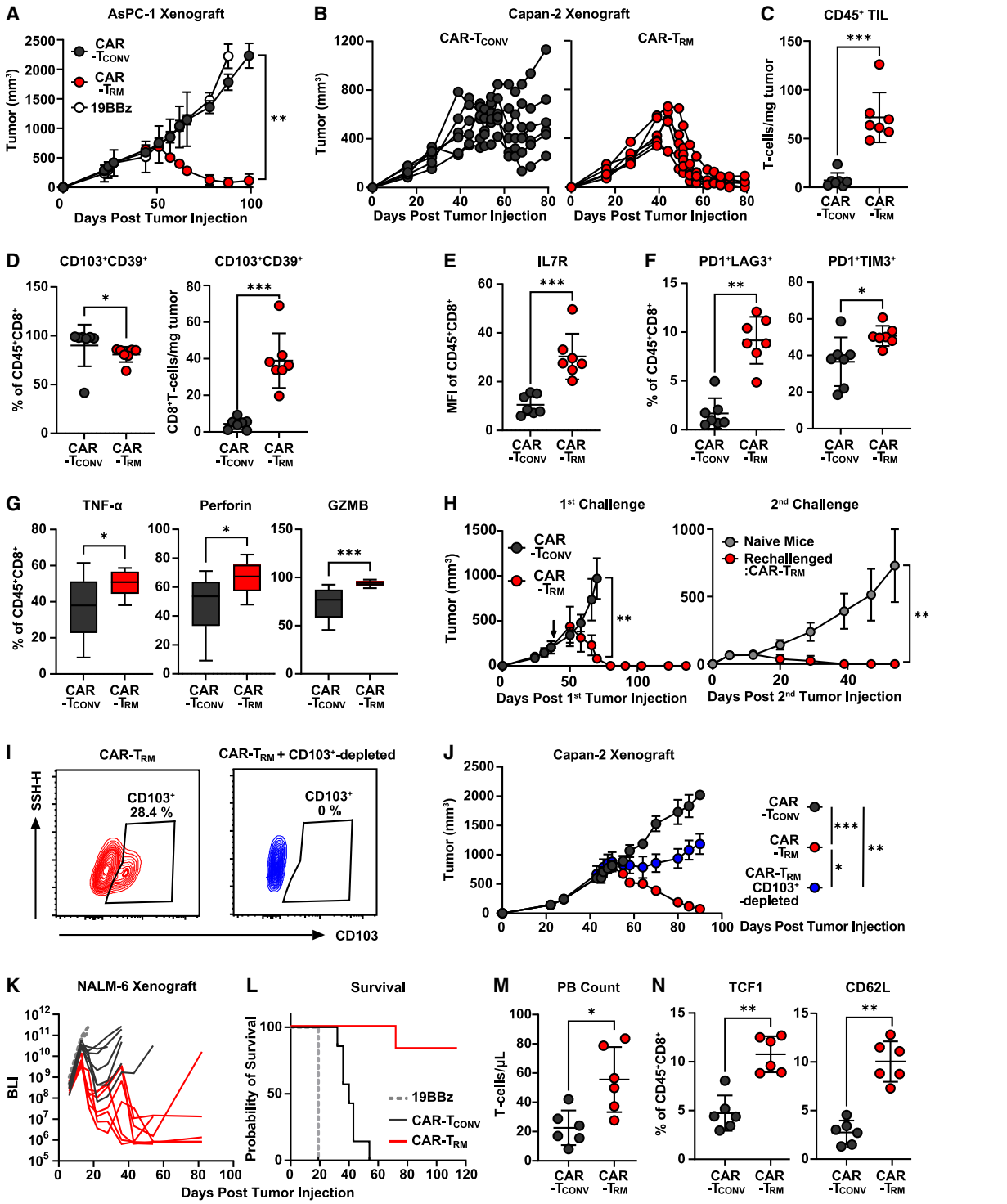

Figure 6. CAR-T_{RM} cells with stem-like features mediated superior antitumor efficacy

(A) NOD scid gamma (NSG) mice were subcutaneously engrafted with 4 × 10^6 AsPC-1 pancreatic cancer cells. On day 32 post tumor implantation, M5 CAR-T_{CONV}, CAR-T_{RM}, or irrelevant (control) CD19-targeting CAR T cells (19BBz) were infused (n = 7 biological replicates for CAR-T_{CONV} and CAR-T_{RM}, n = 2 biological replicates for 19BBz). Tumor size was measured by taking caliper measurements over time.

(B–G) 5 × 10^6 Capan-2 pancreatic adenocarcinoma cells were subcutaneously injected into NSG mice. M5 CAR-T_{CONV} and CAR-T_{RM} were intravenously administered on day 29 following tumor engraftment (n = 6 biological replicates).

(legend continued on next page)

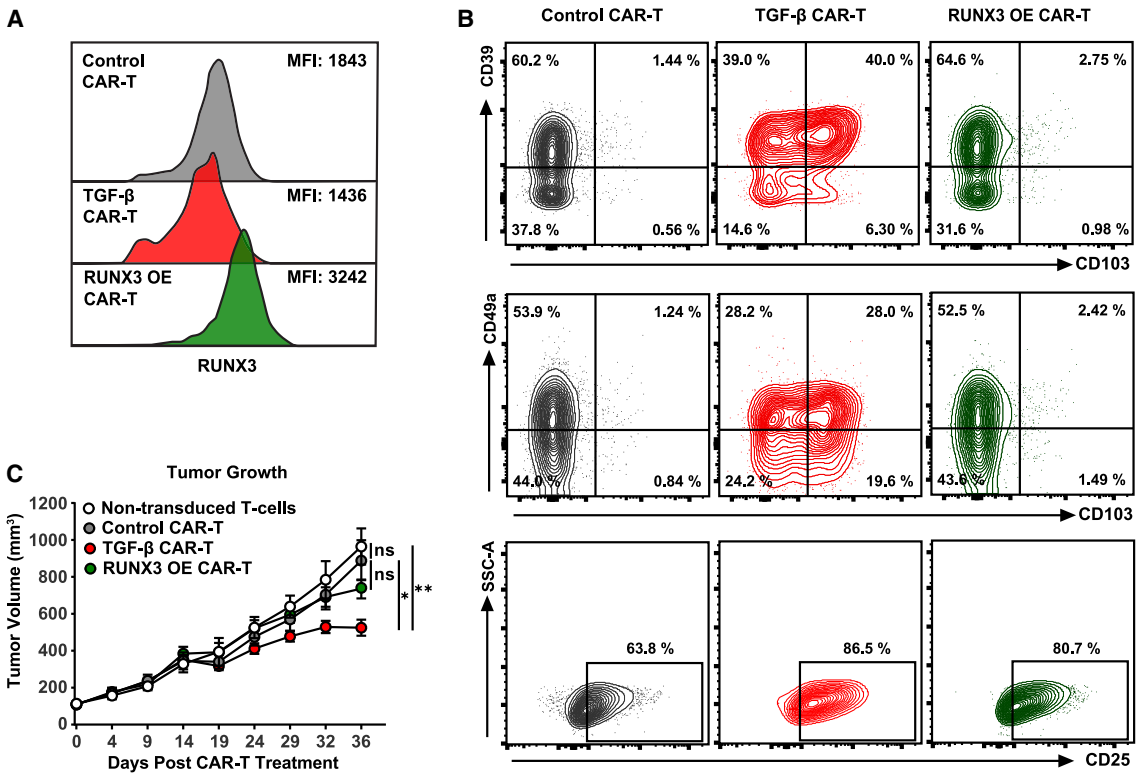

Figure 7. Comparison of CAR-TRM cell differentiation methods

(A) RUNX3 expression measured in various anti-mesothelin SS1 CAR T cell products: standard T cell medium culture (control CAR T), standard T cell medium supplemented with TGF-β (TGF-β CAR T) and engineered to overexpress RUNX3 (RUNX3 OE CAR T) (MFI, geometric mean fluorescence intensity).

(B) T_{RM} (CD103, CD39, CD49a) and activation (CD25) markers were assessed after CAR T cell manufacturing.

(C) NSG mice (n = 7 biological replicates per group) were injected with the EMMESO cell line. Once tumors reached a size of ~120 mm^3, mice received a single dose of 1 × 10^7 SS1 CAR T cells. Activated non-transduced T cells served as a negative control. *p < 0.05; **p < 0.01; ***p < 0.001; ns, not significant (one-way ANOVA).

control, despite exposure to tonic CAR signaling.[84] This suggests that the presence or absence of specific transcription factors alone may not determine the function of CAR T cells, but rather a complex interplay of multiple factors is involved.

These findings suggest that the epigenetic and transcriptional programs of exhausted CAR T cells and CAR-T_{RM} cells are intertwined; however, despite these hallmarks of exhaustion, CAR-T_{RM} cells display enhanced *in vitro* cytokine production compared with conventional CAR T cells and exhibit resistance to cancer-imposed dysfunction, which leads to superior *in vivo* antitumor efficacy. This indicates that certain epigenetic and transcriptional features of classical T cell exhaustion are

(B) Longitudinal tumor growth was monitored. Tumors were collected to characterize the immunophenotype of tumor-infiltrating CAR T cells (Mann-Whitney U test, n = 7 biological replicates).

(C) Absolute number of human T cells in the tumor.

(D) Frequency (left) and absolute number (right) of $CD103^+CD39^+CD8^+$ T cells in harvested tumors.

(E and F) Frequencies of $hCD45^+CD8^+$ cells expressing (E) IL7R and (F) PD1, LAG3, and TIM3.

(G) Tumor-infiltrating CAR T cells were reactivated ionomycin and phorbol 12-myristate 13-acetate and ionomycin, followed by measurement of effector molecule (TNFα, perforin, granzyme B) production.

(H) 4 × 10^6 Capan-2 cells were subcutaneously inoculated into NSG mice that had cleared an initial Capan-2 tumor and had survived until day 138 (left) or into CAR T-naive mice as a control group. Longitudinal tumor growth after the second tumor challenge was monitored (right).

(I) Flow cytometry plots showing CD103 expression on CAR-T_{RM} cells with or without magnetic depletion of $CD103^+$ cells.

(J) CAR-T_{CONV}, CAR-T_{RM}, and $CD103^+$ cell-depleted CAR-T_{RM} cells were intravenously administered to NSG mice harboring subcutaneous Capan-2 tumors. Tumor growth was monitored over time (Mann-Whitney U test, n = 7 biological replicates).

(K–N) 10^6 NALM6 B cell leukemia cells were intravenously injected into NSG mice, and anti-CD19 CAR T cells were infused on day seven.

(K) Tumor growth measured by bioluminescent imaging is shown.

(L) Kaplan-Meier curves depicting survival of mice (log rank test). On day 12 after CAR T cell injection, peripheral blood samples were collected for T cell immunophenotyping.

(M) Peripheral blood human T cell count is shown.

(N) Expression of early memory markers (TCF1, CD62L). All *in vivo* efficacy data are representative of two independent experiments. *p < 0.05; *p < 0.01; ***p < 0.001; ns., not significant.

decoupled from CAR-T_{RM} cell functionality. Furthermore, we identified IRF4 as a transcription factor implicated in both exhaustion and residency programming, specifically regulating exhaustion without promoting a resident memory phenotype. Our study of transcription factor KOs thus provides valuable insight into the co-regulation of tissue-residency and exhaustion pathways and indicates that exhaustion and tissue-residency features may be uncoupled for further improvement of CAR-T_{RM} cells.

In conclusion, our study demonstrates the potential of CAR-T_{RM} cells to overcome the limitations of current CAR T cell therapies by providing a source of immune cells with enhanced tumor accumulation and sustained resistance to dysfunction. Our study also provides a straightforward and practical method for generating these human stem-like CAR-T_{RM} cells, which stands apart from previous attempts to create resident memory cells in murine T cells (e.g., RUNX3 transcription factor overexpression[31] or Von Hippel Lindau [VHL] knockout[44] methods). Our findings also provide valuable insights into the regulation of tissue-residency and exhaustion pathways in human T_{RM} cells and how these two features can be uncoupled for further improvement of CAR-T_{RM}-based therapies. Thus, this work collectively supports the use of TGF-β-generated CAR-T_{RM} cells in early-phase clinical trials currently underway at our center, with the potential to revolutionize the treatment of various diseases, including infectious diseases, autoimmunity, and cardiac disease.

Limitations of the study

Potential limitations of our study include the use of xenograft models for human T cells, lacking the presence of host-derived cells such as regulatory T cells and myeloid-derived suppressor cells, which may affect the results. To better reflect human pathophysiology, further testing of CAR-T_{RM} cells in immunocompetent models is required. However, transitioning to an immunocompetent model would necessitate the use of mouse T cells, which exhibit numerous dissimilarities from their human counterparts. Despite these limitations, xenogeneic mouse models still provide good methods for assessment of potential CAR T cell-augmenting strategies, with subsequent direct testing in humans being critical. The pleiotropic roles of TGF-β in CAR T cell therapy should also be further examined in the future, as previous studies have shown that TGF-β inhibition and ICB produce the best responses and T cell reinvigoration.[85,86] In addition, our proposed strategy must be evaluated in light of previous research that demonstrates the enhancement of antitumor function through blocking TGF-β signaling in CAR T cells.[42,87–89] Notably, our findings indicate that exposure to TGF-β during the manufacturing process of CAR T cells, optimized for concentration and exposure time, leads to an epigenetic reprogramming that enforces a durable T cell tissue-residency state without compromising antitumor immunity. Thus, while our study has some limitations, it provides a foundation for further exploring the potential of CAR-T_{RM} cells as a promising therapy for various diseases.

STAR★METHODS

Detailed methods are provided in the online version of this paper and include the following:

- KEY RESOURCES TABLE
- RESOURCE AVAILABILITY
  - Lead contact
  - Materials availability
  - Data and code availability
- EXPERIMENTAL MODEL AND SUBJECT DETAILS
  - Cell lines
  - Primary human T-cells
  - Mice
- METHOD DETAILS
  - Lentivirus production
  - T-cell culture and lentiviral transduction
  - Gene editing using CRISPR/Cas9
  - Flow cytometry
  - *In vitro* restimulation assay
  - Cytotoxicity assay
  - Mouse xenograft studies
  - Bulk RNA-seq
  - Single-cell RNA sequencing
  - ATAC-seq analysis
  - Statistical analyses

SUPPLEMENTAL INFORMATION

Supplemental information can be found online at https://doi.org/10.1016/j.xcrm.2023.101053.

ACKNOWLEDGMENTS

The authors gratefully acknowledge the Human Immunology Core for providing leukocytes, the Hospital of the University of Pennsylvania Apheresis Unit for peripheral blood mononuclear cell collections, and the Stem Cell and Xenograft Core for their valuable assistance with mouse studies, all at the University of Pennsylvania. We would like to extend our gratitude to Dr. Krishnendu Roy from the Georgia Institute of Technology for his valuable feedback and insightful suggestions, which greatly contributed to the improvement of our work. This project was supported by a National Science Foundation Engineering Research Center for Cell Manufacturing Technologies grant (EEC1648035; to B.L.L. and J.A.F.), the Bob Levis Funding Group (to B.L.L. and J.A.F.), a Prostate Cancer Foundation Tactical Award (to J.A.F.), an Alliance for Cancer Gene Therapy Investigator Award in Cell and Gene Therapy for Cancer (to J.A.F.), U54 CA244711 (to M.M.D. and J.A.F.), P01 CA214278 (to M.M.D. and J.A.F.), U01 AG066100 (to J.A.F.), a Samuel Waxman Cancer Research Foundation Grant (to J.A.F.), and an ACC P30 Core Grant P30 CA016520-42 (to J.A.F.). The graphical abstract was generated using BioRender.com.

AUTHOR CONTRIBUTIONS

Conceptualization, I.Y.J., E.K.M., S.M.A., and J.A.F.; methodology, I.Y.J., E.N.O., E.K.M., S.M.A., and J.A.F.; investigation, I.Y.J., E.N.O., R.B., S.M.C., E.W., M.D., J.K.J., G.P., D.L.S., A.C., B.L.L., S.L.B., E.K.M., S.M.A., and J.A.F.; writing – original draft, I.Y.J. and J.A.F.; writing – review and editing, I.Y.J., E.N.O., S.M.A., and J.A.F.; supervision, S.M.A. and J.A.F.; project administration, S.M.A. and J.A.F.; funding acquisition, J.A.F.

DECLARATION OF INTERESTS

I.Y.J., D.L.S., M.M.D., A.C., B.L.L., E.K.M., S.M.A., and J.A.F. hold patents and intellectual property related to T cell-based cancer immunotherapy and have received royalties. M.M.D. has obtained research funding from Tmunity Therapeutics and is a member of the Scientific Advisory Board for Cellares Corporation. A.C. is a co-founder and has equity in Tmunity Therapeutics. B.L.L.

serves as a consultant for Terumo and GSK; is on the Scientific Advisory Boards for Akron, Avectas, Immuneel, Immusoft, In8bio, Ori Biotech, Oxford Biomedica, and Vycellix; and holds equity as a co-founder in both Tmunity Therapeutics and Capstan Therapeutics. S.M.A. is a co-founder and equity holder in Capstan Therapeutics. J.A.F. receives research funding from Tmunity Therapeutics and Danaher Corporation, consults for Retro Biosciences, and is a member of the Scientific Advisory Boards for Cartography Bio and Shennon Biotechnologies Inc.

INCLUSION AND DIVERSITY

We support inclusive, diverse, and equitable conduct of research.

Received: November 1, 2022
Revised: February 21, 2023
Accepted: April 27, 2023
Published: May 23, 2023

REFERENCES

1. Maude, S.L., Laetsch, T.W., Buechner, J., Rives, S., Boyer, M., Bittencourt, H., Bader, P., Verneris, M.R., Stefanski, H.E., Myers, G.D., et al. (2018). Tisagenlecleucel in children and young adults with B-cell lymphoblastic leukemia. N. Engl. J. Med. *378*, 439–448. https://doi.org/10.1056/NEJMoa1709866.
2. Park, J.H., Rivière, I., Gonen, M., Wang, X., Sénéchal, B., Curran, K.J., Sauter, C., Wang, Y., Santomasso, B., Mead, E., et al. (2018). Long-term follow-up of CD19 CAR therapy in acute lymphoblastic leukemia. N. Engl. J. Med. *378*, 449–459. https://doi.org/10.1056/NEJMoa1709919.
3. Schuster, S.J., Bishop, M.R., Tam, C.S., Waller, E.K., Borchmann, P., McGuirk, J.P., Jäger, U., Jaglowski, S., Andreadis, C., Westin, J.R., et al. (2019). Tisagenlecleucel in adult relapsed or refractory diffuse large B-cell lymphoma. N. Engl. J. Med. *380*, 45–56. https://doi.org/10.1056/NEJMoa1804980.
4. Locke, F.L., Miklos, D.B., Jacobson, C.A., Perales, M.A., Kersten, M.J., Oluwole, O.O., Ghobadi, A., Rapoport, A.P., McGuirk, J., Pagel, J.M., et al. (2022). Axicabtagene ciloleucel as second-line therapy for large B-cell lymphoma. N. Engl. J. Med. *386*, 640–654. https://doi.org/10.1056/NEJMoa2116133.
5. Wang, M., Munoz, J., Goy, A., Locke, F.L., Jacobson, C.A., Hill, B.T., Timmerman, J.M., Holmes, H., Jaglowski, S., Flinn, I.W., et al. (2020). KTE-X19 CAR T-cell therapy in relapsed or refractory mantle-cell lymphoma. N. Engl. J. Med. *382*, 1331–1342. https://doi.org/10.1056/NEJMoa1914347.
6. Raje, N., Berdeja, J., Lin, Y., Siegel, D., Jagannath, S., Madduri, D., Liedtke, M., Rosenblatt, J., Maus, M.V., Turka, A., et al. (2019). Anti-BCMA CAR T-cell therapy bb2121 in relapsed or refractory multiple myeloma. N. Engl. J. Med. *380*, 1726–1737. https://doi.org/10.1056/NEJMoa1817226.
7. Munshi, N.C., Anderson, L.D., Jr., Shah, N., Madduri, D., Berdeja, J., Lonial, S., Raje, N., Lin, Y., Siegel, D., Oriol, A., et al. (2021). Idecabtagene vicleucel in relapsed and refractory multiple myeloma. N. Engl. J. Med. *384*, 705–716. https://doi.org/10.1056/NEJMoa2024850.
8. Mailankody, S., Devlin, S.M., Landa, J., Nath, K., Diamonte, C., Carstens, E.J., Russo, D., Auclair, R., Fitzgerald, L., Cadzin, B., et al. (2022). GPRC5D-Targeted CAR T cells for myeloma. N. Engl. J. Med. *387*, 1196–1206. https://doi.org/10.1056/NEJMoa2209900.
9. Siegel, R.L., Miller, K.D., Fuchs, H.E., and Jemal, A. (2022). Cancer statistics, 2022. CA. Cancer J. Clin. *72*, 7–33. https://doi.org/10.3322/caac.21708.
10. Nguyen, D.T., Ogando-Rivas, E., Liu, R., Wang, T., Rubin, J., Jin, L., Tao, H., Sawyer, W.W., Mendez-Gomez, H.R., Cascio, M., et al. (2022). CAR T cell locomotion in solid tumor microenvironment. Cells *11*. https://doi.org/10.3390/cells11121974.
11. Martinez, M., and Moon, E.K. (2019). CAR T cells for solid tumors: new strategies for finding, infiltrating, and surviving in the tumor microenvironment. Front. Immunol. *10*, 128. https://doi.org/10.3389/fimmu.2019.00128.
12. Craddock, J.A., Lu, A., Bear, A., Pule, M., Brenner, M.K., Rooney, C.M., and Foster, A.E. (2010). Enhanced tumor trafficking of GD2 chimeric antigen receptor T cells by expression of the chemokine receptor CCR2b. J. Immunother. *33*, 780–788. https://doi.org/10.1097/CJI.0b013e3181ee6675.
13. Moon, E.K., Carpenito, C., Sun, J., Wang, L.C.S., Kapoor, V., Predina, J., Powell, D.J., Jr., Riley, J.L., June, C.H., and Albelda, S.M. (2011). Expression of a functional CCR2 receptor enhances tumor localization and tumor eradication by retargeted human T cells expressing a mesothelin-specific chimeric antibody receptor. Clin. Cancer Res. *17*, 4719–4730. https://doi.org/10.1158/1078-0432.CCR-11-0351.
14. Xie, Y.J., Dougan, M., Jailkhani, N., Ingram, J., Fang, T., Kummer, L., Momin, N., Pishesha, N., Rickelt, S., Hynes, R.O., and Ploegh, H. (2019). Nanobody-based CAR T cells that target the tumor microenvironment inhibit the growth of solid tumors in immunocompetent mice. Proc. Natl. Acad. Sci. USA *116*, 7624–7631. https://doi.org/10.1073/pnas.1817147116.
15. Majzner, R.G., and Mackall, C.L. (2018). Tumor antigen escape from CAR T-cell therapy. Cancer Discov. *8*, 1219–1226. https://doi.org/10.1158/2159-8290.CD-18-0442.
16. O'Rourke, D.M., Nasrallah, M.P., Desai, A., Melenhorst, J.J., Mansfield, K., Morrissette, J.J.D., Martinez-Lage, M., Brem, S., Maloney, E., Shen, A., et al. (2017). A single dose of peripherally infused EGFRvIII-directed CAR T cells mediates antigen loss and induces adaptive resistance in patients with recurrent glioblastoma. Sci. Transl. Med. *9*, eaaa0984. https://doi.org/10.1126/scitranslmed.aaa0984.
17. Majzner, R.G., Ramakrishna, S., Yeom, K.W., Patel, S., Chinnasamy, H., Schultz, L.M., Richards, R.M., Jiang, L., Barsan, V., Mancusi, R., et al. (2022). GD2-CAR T cell therapy for H3K27M-mutated diffuse midline gliomas. Nature *603*, 934–941. https://doi.org/10.1038/s41586-022-04489-4.
18. Tang, O.Y., Tian, L., Yoder, T., Xu, R., Kulikovskaya, I., Gupta, M., Melenhorst, J.J., Lacey, S.F., O'Rourke, D.M., and Binder, Z.A. (2022). PD1 expression in EGFRvIII-directed CAR T cell infusion product for glioblastoma is associated with clinical response. Front. Immunol. *13*, 872756. https://doi.org/10.3389/fimmu.2022.872756.
19. Jung, I.Y., Narayan, V., McDonald, S., Rech, A.J., Bartoszek, R., Hong, G., Davis, M.M., Xu, J., Boesteanu, A.C., Barber-Rotenberg, J.S., et al. (2022). BLIMP1 and NR4A3 transcription factors reciprocally regulate antitumor CAR T-cell stemness and exhaustion science. Trans Med *14*, eabn7336. In Press.
20. Guo, A., Huang, H., Zhu, Z., Chen, M.J., Shi, H., Yuan, S., Sharma, P., Connelly, J.P., Liedmann, S., Dhungana, Y., et al. (2022). cBAF complex components and MYC cooperate early in CD8(+) T cell fate. Nature *607*, 135–141. https://doi.org/10.1038/s41586-022-04849-0.
21. Gattinoni, L., Lugli, E., Ji, Y., Pos, Z., Paulos, C.M., Quigley, M.F., Almeida, J.R., Gostick, E., Yu, Z., Carpenito, C., et al. (2011). A human memory T cell subset with stem cell-like properties. Nat. Med. *17*, 1290–1297. https://doi.org/10.1038/nm.2446.
22. Masopust, D., Vezys, V., Marzo, A.L., and Lefrançois, L. (2001). Preferential localization of effector memory cells in nonlymphoid tissue. Science *291*, 2413–2417. https://doi.org/10.1126/science.1058867.
23. Hogan, R.J., Zhong, W., Usherwood, E.J., Cookenham, T., Roberts, A.D., and Woodland, D.L. (2001). Protection from respiratory virus infections can be mediated by antigen-specific CD4(+) T cells that persist in the lungs. J. Exp. Med. *193*, 981–986. https://doi.org/10.1084/jem.193.8.981.
24. Gebhardt, T., Wakim, L.M., Eidsmo, L., Reading, P.C., Heath, W.R., and Carbone, F.R. (2009). Memory T cells in nonlymphoid tissue that provide enhanced local immunity during infection with herpes simplex virus. Nat. Immunol. *10*, 524–530. https://doi.org/10.1038/ni.1718.
25. Wakim, L.M., Waithman, J., van Rooijen, N., Heath, W.R., and Carbone, F.R. (2008). Dendritic cell-induced memory T cell activation in nonlymphoid tissues. Science *319*, 198–202. https://doi.org/10.1126/science.1151869.

26. Zheng, L., Qin, S., Si, W., Wang, A., Xing, B., Gao, R., Ren, X., Wang, L., Wu, X., Zhang, J., et al. (2021). Pan-cancer single-cell landscape of tumor-infiltrating T cells. Science *374*, abe6474. https://doi.org/10.1126/science.abe6474.

27. Edwards, J., Wilmott, J.S., Madore, J., Gide, T.N., Quek, C., Tasker, A., Ferguson, A., Chen, J., Hewavisenti, R., Hersey, P., et al. (2018). CD103(+) tumor-resident CD8(+) T cells are associated with improved survival in immunotherapy-naive melanoma patients and expand significantly during anti-PD-1 treatment. Clin. Cancer Res. *24*, 3036–3045. https://doi.org/10.1158/1078-0432.CCR-17-2257.

28. Bösmüller, H.C., Wagner, P., Peper, J.K., Schuster, H., Pham, D.L., Greif, K., Beschorner, C., Rammensee, H.G., Stevanović, S., Fend, F., and Staebler, A. (2016). Combined immunoscore of CD103 and CD3 identifies long-term survivors in high-grade serous ovarian cancer. Int. J. Gynecol. Cancer *26*, 671–679. https://doi.org/10.1097/IGC.0000000000000672.

29. Workel, H.H., Komdeur, F.L., Wouters, M.C.A., Plat, A., Klip, H.G., Eggink, F.A., Wisman, G.B.A., Arts, H.J.G., Oonk, M.H.M., Mourits, M.J.E., et al. (2016). CD103 defines intraepithelial CD8+ PD1+ tumour-infiltrating lymphocytes of prognostic significance in endometrial adenocarcinoma. Eur. J. Cancer *60*, 1–11. https://doi.org/10.1016/j.ejca.2016.02.026.

30. Skon, C.N., Lee, J.Y., Anderson, K.G., Masopust, D., Hogquist, K.A., and Jameson, S.C. (2013). Transcriptional downregulation of S1pr1 is required for the establishment of resident memory CD8+ T cells. Nat. Immunol. *14*, 1285–1293. https://doi.org/10.1038/ni.2745.

31. Milner, J.J., Toma, C., Yu, B., Zhang, K., Omilusik, K., Phan, A.T., Wang, D., Getzler, A.J., Nguyen, T., Crotty, S., et al. (2017). Runx3 programs CD8(+) T cell residency in non-lymphoid tissues and tumours. Nature *552*, 253–257. https://doi.org/10.1038/nature24993.

32. Holz, L.E., Prier, J.E., Freestone, D., Steiner, T.M., English, K., Johnson, D.N., Mollard, V., Cozijnsen, A., Davey, G.M., Godfrey, D.I., et al. (2018). CD8(+) T cell activation leads to constitutive formation of liver tissue-resident memory T cells that seed a large and flexible niche in the liver. Cell Rep. *25*, 68–79.e4. https://doi.org/10.1016/j.celrep.2018.08.094.

33. Szabo, P.A., Miron, M., and Farber, D.L. (2019). Location, location, location: tissue resident memory T cells in mice and humans. Sci. Immunol. *4*, eaas9673. https://doi.org/10.1126/sciimmunol.aas9673.

34. Milner, J.J., Toma, C., He, Z., Kurd, N.S., Nguyen, Q.P., McDonald, B., Quezada, L., Widjaja, C.E., Witherden, D.A., Crowl, J.T., et al. (2020). Heterogenous populations of tissue-resident CD8(+) T cells are generated in response to infection and malignancy. Immunity *52*, 808–824.e7. https://doi.org/10.1016/j.immuni.2020.04.007.

35. Li, G., Srinivasan, S., Wang, L., Ma, C., Guo, K., Xiao, W., Liao, W., Mishra, S., Zhang, X., Qiu, Y., et al. (2022). TGF-beta-dependent lymphoid tissue residency of stem-like T cells limits response to tumor vaccine. Nat. Commun. *13*, 6043. https://doi.org/10.1038/s41467-022-33768-x.

36. Kurtulus, S., Madi, A., Escobar, G., Klapholz, M., Nyman, J., Christian, E., Pawlak, M., Dionne, D., Xia, J., Rozenblatt-Rosen, O., et al. (2019). Checkpoint blockade immunotherapy induces dynamic changes in PD-1(-) CD8(+) tumor-infiltrating T cells. Immunity *50*, 181–194.e6. https://doi.org/10.1016/j.immuni.2018.11.014.

37. Casey, K.A., Fraser, K.A., Schenkel, J.M., Moran, A., Abt, M.C., Beura, L.K., Lucas, P.J., Artis, D., Wherry, E.J., Hogquist, K., et al. (2012). Antigen-independent differentiation and maintenance of effector-like resident memory T cells in tissues. J. Immunol. *188*, 4866–4875. https://doi.org/10.4049/jimmunol.1200402.

38. Mackay, L.K., Rahimpour, A., Ma, J.Z., Collins, N., Stock, A.T., Hafon, M.L., Vega-Ramos, J., Lauzurica, P., Mueller, S.N., Stefanovic, T., et al. (2013). The developmental pathway for CD103(+)CD8+ tissue-resident memory T cells of skin. Nat. Immunol. *14*, 1294–1301. https://doi.org/10.1038/ni.2744.

39. Zhang, N., and Bevan, M.J. (2013). Transforming growth factor-beta signaling controls the formation and maintenance of gut-resident memory T cells by regulating migration and retention. Immunity *39*, 687–696. https://doi.org/10.1016/j.immuni.2013.08.019.

40. Ganesan, A.P., Clarke, J., Wood, O., Garrido-Martin, E.M., Chee, S.J., Mellows, T., Samaniego-Castruita, D., Singh, D., Seumois, G., Alzetani, A., et al. (2017). Tissue-resident memory features are linked to the magnitude of cytotoxic T cell responses in human lung cancer. Nat. Immunol. *18*, 940–950. https://doi.org/10.1038/ni.3775.

41. Hombrink, P., Helbig, C., Backer, R.A., Piet, B., Oja, A.E., Stark, R., Brasser, G., Jongejan, A., Jonkers, R.E., Nota, B., et al. (2016). Programs for the persistence, vigilance and control of human CD8(+) lung-resident memory T cells. Nat. Immunol. *17*, 1467–1478. https://doi.org/10.1038/ni.3589.

42. Kloss, C.C., Lee, J., Zhang, A., Chen, F., Melenhorst, J.J., Lacey, S.F., Maus, M.V., Fraietta, J.A., Zhao, Y., and June, C.H. (2018). Dominant-negative TGF-beta receptor enhances PSMA-targeted human CAR T cell proliferation and augments prostate cancer eradication. Mol. Ther. *26*, 1855–1866. https://doi.org/10.1016/j.ymthe.2018.05.003.

43. Dahmani, A., and Delisle, J.S. (2018). TGF-beta in T Cell biology: implications for cancer immunotherapy. Cancers *10*, 194. https://doi.org/10.3390/cancers10060194.

44. Liikanen, I., Lauhan, C., Quon, S., Omilusik, K., Phan, A.T., Bartrolí, L.B., Ferry, A., Goulding, J., Chen, J., Scott-Browne, J.P., et al. (2021). Hypoxia-inducible factor activity promotes antitumor effector function and tissue residency by CD8+ T cells. J. Clin. Invest. *131*, e143729. https://doi.org/10.1172/JCI143729.

45. Good, Z., Spiegel, J.Y., Sahaf, B., Malipatlolla, M.B., Ehlinger, Z.J., Kurra, S., Desai, M.H., Reynolds, W.D., Wong Lin, A., Vandris, P., et al. (2022). Post-infusion CAR T(Reg) cells identify patients resistant to CD19-CAR therapy. Nat. Med. *28*, 1860–1871. https://doi.org/10.1038/s41591-022-01960-7.

46. Haradhvala, N.J., Leick, M.B., Maurer, K., Gohil, S.H., Larson, R.C., Yao, N., Gallagher, K.M.E., Katsis, K., Frigault, M.J., Southard, J., et al. (2022). Distinct cellular dynamics associated with response to CAR-T therapy for refractory B cell lymphoma. Nat. Med. *28*, 1848–1859. https://doi.org/10.1038/s41591-022-01959-0.

47. Hou, A.J., Chang, Z.L., Lorenzini, M.H., Zah, E., and Chen, Y.Y. (2018). TGF-beta-responsive CAR-T cells promote anti-tumor immune function. Bioeng. Transl. Med. *3*, 75–86. https://doi.org/10.1002/btm2.10097.

48. Hasan, F., Chiu, Y., Shaw, R.M., Wang, J., and Yee, C. (2021). Hypoxia acts as an environmental cue for the human tissue-resident memory T cell differentiation program. JCI Insight *6*, e138970. https://doi.org/10.1172/jci.insight.138970.

49. Luoma, A.M., Suo, S., Wang, Y., Gunasti, L., Porter, C.B.M., Nabilsi, N., Tadros, J., Ferretti, A.P., Liao, S., Gurer, C., et al. (2022). Tissue-resident memory and circulating T cells are early responders to pre-surgical cancer immunotherapy. Cell *185*, 2918–2935.e29. https://doi.org/10.1016/j.cell.2022.06.018.

50. Gabriel, S.S., Tsui, C., Chisanga, D., Weber, F., Llano-León, M., Gubser, P.M., Bartholin, L., Souza-Fonseca-Guimaraes, F., Huntington, N.D., Shi, W., et al. (2021). Transforming growth factor-beta-regulated mTOR activity preserves cellular metabolism to maintain long-term T cell responses in chronic infection. Immunity *54*, 1698–1714.e5. https://doi.org/10.1016/j.immuni.2021.06.007.

51. Im, S.J., Hashimoto, M., Gerner, M.Y., Lee, J., Kissick, H.T., Burger, M.C., Shan, Q., Hale, J.S., Lee, J., Nasti, T.H., et al. (2016). Defining CD8+ T cells that provide the proliferative burst after PD-1 therapy. Nature *537*, 417–421. https://doi.org/10.1038/nature19330.

52. Caushi, J.X., Zhang, J., Ji, Z., Vaghasia, A., Zhang, B., Hsiue, E.H.C., Mog, B.J., Hou, W., Justesen, S., Blosser, R., et al. (2021). Transcriptional programs of neoantigen-specific TIL in anti-PD-1-treated lung cancers. Nature *596*, 126–132. https://doi.org/10.1038/s41586-021-03752-4.

53. Pauken, K.E., Sammons, M.A., Odorizzi, P.M., Manne, S., Godec, J., Khan, O., Drake, A.M., Chen, Z., Sen, D.R., Kurachi, M., et al. (2016). Epigenetic stability of exhausted T cells limits durability of reinvigoration by PD-1 blockade. Science *354*, 1160–1165. https://doi.org/10.1126/science.aaf2807.

54. Araki, Y., Fann, M., Wersto, R., and Weng, N.P. (2008). Histone acetylation facilitates rapid and robust memory CD8 T cell response through differential expression of effector molecules (eomesodermin and its targets: perforin and granzyme B). J. Immunol. *180*, 8102–8108. https://doi.org/10.4049/jimmunol.180.12.8102.

55. Araki, Y., Wang, Z., Zang, C., Wood, W.H., 3rd, Schones, D., Cui, K., Roh, T.Y., Lhotsky, B., Wersto, R.P., Peng, W., et al. (2009). Genome-wide analysis of histone methylation reveals chromatin state-based regulation of gene transcription and function of memory CD8+ T cells. Immunity *30*, 912–925. https://doi.org/10.1016/j.immuni.2009.05.006.

56. Petrie, H.T., and Zúñiga-Pflücker, J.C. (2007). Zoned out: functional mapping of stromal signaling microenvironments in the thymus. Annu. Rev. Immunol. *25*, 649–679. https://doi.org/10.1146/annurev.immunol.23.021704.115715.

57. Wherry, E.J. (2011). T cell exhaustion. Nat. Immunol. *12*, 492–499. https://doi.org/10.1038/ni.2035.

58. Doering, T.A., Crawford, A., Angelosanto, J.M., Paley, M.A., Ziegler, C.G., and Wherry, E.J. (2012). Network analysis reveals centrally connected genes and pathways involved in CD8+ T cell exhaustion versus memory. Immunity *37*, 1130–1144. https://doi.org/10.1016/j.immuni.2012.08.021.

59. Schietinger, A., and Greenberg, P.D. (2014). Tolerance and exhaustion: defining mechanisms of T cell dysfunction. Trends Immunol. *35*, 51–60. https://doi.org/10.1016/j.it.2013.10.001.

60. Schøller, A.S., Nazerai, L., Christensen, J.P., and Thomsen, A.R. (2020). Functionally competent, PD-1(+) CD8(+) trm cells populate the brain following local antigen encounter. Front. Immunol. *11*, 595707. https://doi.org/10.3389/fimmu.2020.595707.

61. Lynn, R.C., Weber, E.W., Sotillo, E., Gennert, D., Xu, P., Good, Z., Anbunathan, H., Lattin, J., Jones, R., Tieu, V., et al. (2019). c-Jun overexpression in CAR T cells induces exhaustion resistance. Nature *576*, 293–300. https://doi.org/10.1038/s41586-019-1805-z.

62. Dai, X., Park, J.J., Du, Y., Na, Z., Lam, S.Z., Chow, R.D., Renauer, P.A., Gu, J., Xin, S., Chu, Z., et al. (2023). Massively parallel knock-in engineering of human T cells. Preprint at Nat. Biotechnol. https://doi.org/10.1038/s41587-022-01639-x.

63. Yoshikawa, T., Wu, Z., Inoue, S., Kasuya, H., Matsushita, H., Takahashi, Y., Kuroda, H., Hosoda, W., Suzuki, S., and Kagoya, Y. (2022). Genetic ablation of PRDM1 in antitumor T cells enhances therapeutic efficacy of adoptive immunotherapy. Blood *139*, 2156–2172. https://doi.org/10.1182/blood.2021012714.

64. Omilusik, K.D., Nadjsombati, M.S., Shaw, L.A., Yu, B., Milner, J.J., and Goldrath, A.W. (2018). Sustained Id2 regulation of E proteins is required for terminal differentiation of effector CD8(+) T cells. J. Exp. Med. *215*, 773–783. https://doi.org/10.1084/jem.20171584.

65. Masson, F., Minnich, M., Olshansky, M., Bilic, I., Mount, A.M., Kallies, A., Speed, T.P., Busslinger, M., Nutt, S.L., and Belz, G.T. (2013). Id2-mediated inhibition of E2A represses memory CD8+ T cell differentiation. J. Immunol. *190*, 4585–4594. https://doi.org/10.4049/jimmunol.1300099.

66. Seo, H., Chen, J., González-Avalos, E., Samaniego-Castruita, D., Das, A., Wang, Y.H., López-Moyado, I.F., Georges, R.O., Zhang, W., Onodera, A., et al. (2019). TOX and TOX2 transcription factors cooperate with NR4A transcription factors to impose CD8(+) T cell exhaustion. Proc. Natl. Acad. Sci. USA *116*, 12410–12415. https://doi.org/10.1073/pnas.1905675116.

67. Utzschneider, D.T., Gabriel, S.S., Chisanga, D., Gloury, R., Gubser, P.M., Vasanthakumar, A., Shi, W., and Kallies, A. (2020). Early precursor T cells establish and propagate T cell exhaustion in chronic infection. Nat. Immunol. *21*, 1256–1266. https://doi.org/10.1038/s41590-020-0760-z.

68. Du, N., Kwon, H., Li, P., West, E.E., Oh, J., Liao, W., Yu, Z., Ren, M., and Leonard, W.J. (2014). EGR2 is critical for peripheral naive T-cell differentiation and the T-cell response to influenza. Proc. Natl. Acad. Sci. USA *111*, 16484–16489. https://doi.org/10.1073/pnas.1417215111.

69. Kurd, N.S., He, Z., Louis, T.L., Milner, J.J., Omilusik, K.D., Jin, W., Tsai, M.S., Widjaja, C.E., Kanbar, J.N., Olvera, J.G., et al. (2020). Early precursors and molecular determinants of tissue-resident memory CD8(+) T lymphocytes revealed by single-cell RNA sequencing. Sci. Immunol. *5*, eaaz6894. https://doi.org/10.1126/sciimmunol.aaz6894.

70. Harberts, A., Schmidt, C., Schmid, J., Reimers, D., Koch-Nolte, F., Mittrücker, H.W., and Raczkowski, F. (2021). Interferon regulatory factor 4 controls effector functions of CD8(+) memory T cells. Proc. Natl. Acad. Sci. USA *118*, e2014553118. https://doi.org/10.1073/pnas.2014553118.

71. Frigault, M.J., Lee, J., Basil, M.C., Carpenito, C., Motohashi, S., Scholler, J., Kawalekar, O.U., Guedan, S., McGettigan, S.E., Posey, A.D., Jr., et al. (2015). Identification of chimeric antigen receptors that mediate constitutive or inducible proliferation of T cells. Cancer Immunol. Res. *3*, 356–367. https://doi.org/10.1158/2326-6066.CIR-14-0186.

72. Moon, E.K., Wang, L.C., Dolfi, D.V., Wilson, C.B., Ranganathan, R., Sun, J., Kapoor, V., Scholler, J., Puré, E., Milone, M.C., et al. (2014). Multifactorial T-cell hypofunction that is reversible can limit the efficacy of chimeric antigen receptor-transduced human T cells in solid tumors. Clin. Cancer Res. *20*, 4262–4273. https://doi.org/10.1158/1078-0432.CCR-13-2627.

73. Haas, A.R., Tanyi, J.L., O'Hara, M.H., Gladney, W.L., Lacey, S.F., Torigian, D.A., Soulen, M.C., Tian, L., McGarvey, M., Nelson, A.M., et al. (2019). Phase I study of lentiviral-transduced chimeric antigen receptor-modified T cells recognizing mesothelin in advanced solid cancers. Mol. Ther. *27*, 1919–1929. https://doi.org/10.1016/j.ymthe.2019.07.015.

74. Oh, S.A., and Li, M.O. (2013). TGF-beta: guardian of T cell function. J. Immunol. *191*, 3973–3979. https://doi.org/10.4049/jimmunol.1301843.

75. Lee, Y.T., Suarez-Ramirez, J.E., Wu, T., Redman, J.M., Bouchard, K., Hadley, G.A., and Cauley, L.S. (2011). Environmental and antigen receptor-derived signals support sustained surveillance of the lungs by pathogen-specific cytotoxic T lymphocytes. J. Virol. *85*, 4085–4094. https://doi.org/10.1128/JVI.02493-10.

76. Cretney, E., Xin, A., Shi, W., Minnich, M., Masson, F., Miasari, M., Belz, G.T., Smyth, G.K., Busslinger, M., Nutt, S.L., and Kallies, A. (2011). The transcription factors Blimp-1 and IRF4 jointly control the differentiation and function of effector regulatory T cells. Nat. Immunol. *12*, 304–311. https://doi.org/10.1038/ni.2006.

77. Li, C., Zhu, B., Son, Y.M., Wang, Z., Jiang, L., Xiang, M., Ye, Z., Beckermann, K.E., Wu, Y., Jenkins, J.W., et al. (2019). The transcription factor Bhlhe40 programs mitochondrial regulation of resident CD8(+) T cell fitness and functionality. Immunity *51*, 491–507.e7. https://doi.org/10.1016/j.immuni.2019.08.013.

78. Zaid, A., Mackay, L.K., Rahimpour, A., Braun, A., Veldhoen, M., Carbone, F.R., Manton, J.H., Heath, W.R., and Mueller, S.N. (2014). Persistence of skin-resident memory T cells within an epidermal niche. Proc. Natl. Acad. Sci. USA *111*, 5307–5312. https://doi.org/10.1073/pnas.1322292111.

79. Mackay, L.K., Wynne-Jones, E., Freestone, D., Pellicci, D.G., Mielke, L.A., Newman, D.M., Braun, A., Masson, F., Kallies, A., Belz, G.T., and Carbone, F.R. (2015). T-Box transcription factors combine with the cytokines TGF-beta and IL-15 to control tissue-resident memory T cell fate. Immunity *43*, 1101–1111. https://doi.org/10.1016/j.immuni.2015.11.008.

80. Fonseca, R., Burn, T.N., Gandolfo, L.C., Devi, S., Park, S.L., Obers, A., Evrard, M., Christo, S.N., Buquicchio, F.A., Lareau, C.A., et al. (2022). Runx3 drives a CD8(+) T cell tissue residency program that is absent in CD4(+) T cells. Nat. Immunol. *23*, 1236–1245. https://doi.org/10.1038/s41590-022-01273-4.

81. Pallett, L.J., Davies, J., Colbeck, E.J., Robertson, F., Hansi, N., Easom, N.J.W., Burton, A.R., Stegmann, K.A., Schurich, A., Swadling, L., et al. (2017). IL-2(high) tissue-resident T cells in the human liver: sentinels for hepatotropic infection. J. Exp. Med. *214*, 1567–1580. https://doi.org/10.1084/jem.20162115.

82. Kumar, B.V., Ma, W., Miron, M., Granot, T., Guyer, R.S., Carpenter, D.J., Senda, T., Sun, X., Ho, S.H., Lerner, H., et al. (2017). Human tissue-resident memory T cells are defined by core transcriptional and functional signatures in lymphoid and mucosal sites. Cell Rep. *20*, 2921–2934. https://doi.org/10.1016/j.celrep.2017.08.078.

83. Mackay, L.K., Minnich, M., Kragten, N.A.M., Liao, Y., Nota, B., Seillet, C., Zaid, A., Man, K., Preston, S., Freestone, D., et al. (2016). Hobit and Blimp1 instruct a universal transcriptional program of tissue residency in lymphocytes. Science *352*, 459–463. https://doi.org/10.1126/science.aad2035.

84. Freitas, K.A., Belk, J.A., Sotillo, E., Quinn, P.J., Ramello, M.C., Malipatlolla, M., Daniel, B., Sandor, K., Klysz, D., Bjelajac, J., et al. (2022). Enhanced T cell effector activity by targeting the Mediator kinase module. Science *378*, eabn5647. https://doi.org/10.1126/science.abn5647.

85. Mariathasan, S., Turley, S.J., Nickles, D., Castiglioni, A., Yuen, K., Wang, Y., Kadel, E.E., III, Koeppen, H., Astarita, J.L., Cubas, R., et al. (2018). TGFbeta attenuates tumour response to PD-L1 blockade by contributing to exclusion of T cells. Nature *554*, 544–548. https://doi.org/10.1038/nature25501.

86. Tauriello, D.V.F., Palomo-Ponce, S., Stork, D., Berenguer-Llergo, A., Badia-Ramentol, J., Iglesias, M., Sevillano, M., Ibiza, S., Cañellas, A., Hernando-Momblona, X., et al. (2018). TGFbeta drives immune evasion in genetically reconstituted colon cancer metastasis. Nature *554*, 538–543. https://doi.org/10.1038/nature25492.

87. Tang, N., Cheng, C., Zhang, X., Qiao, M., Li, N., Mu, W., Wei, X.F., Han, W., and Wang, H. (2020). TGF-beta inhibition via CRISPR promotes the long-term efficacy of CAR T cells against solid tumors. JCI Insight *5*, e133977. https://doi.org/10.1172/jci.insight.133977.

88. Narayan, V., Barber-Rotenberg, J.S., Jung, I.Y., Lacey, S.F., Rech, A.J., Davis, M.M., Hwang, W.T., Lal, P., Carpenter, E.L., Maude, S.L., et al. (2022). PSMA-targeting TGFbeta-insensitive armored CAR T cells in metastatic castration-resistant prostate cancer: a phase 1 trial. Nat. Med. *28*, 724–734. https://doi.org/10.1038/s41591-022-01726-1.

89. Stüber, T., Monjezi, R., Wallstabe, L., Kühnemundt, J., Nietzer, S.L., Dandekar, G., Wöckel, A., Einsele, H., Wischhusen, J., and Hudecek, M. (2020). Inhibition of TGF-beta-receptor signaling augments the antitumor function of ROR1-specific CAR T-cells against triple-negative breast cancer. J. Immunother. Cancer *8*, e000676. https://doi.org/10.1136/jitc-2020-000676.

STAR★METHODS

KEY RESOURCES TABLE

REAGENT or RESOURCE	SOURCE	IDENTIFIER
Antibodies		
Brilliant Violet (BV) 421 anti-human CD279 (PD-1)	BioLegend	Cat# 329920; RRID: AB_10960742
BV 711 anti-human CD39	BioLegend	Cat# 328228; RRID: AB_2632894
BV 570 anti-human CD45RO	BioLegend	Cat# 304225; RRID: AB_11126987
BV 650 anti-human CD8a	BioLegend	Cat# 301041; RRID: AB_11125174
BV 785 anti-human CD4	BioLegend	Cat# 317442; RRID: AB_2563242
BV 570 anti-human CD127 (IL-7Ralpha)	BioLegend	Cat# 351308; RRID: AB_2832685
BV 570 anti-human IFN-gamma	BioLegend	Cat# 502534; RRID: AB_2563880
BV 421 anti-human Perforin	BioLegend	Cat# 353307; RRID: AB_11149688
Allophycocyanin (APC) anti-human Perforin	BioLegend	Cat# 308112; RRID: AB_2252843
Alexa Fluor (AF) 700 anti-human TNF-alpha	BioLegend	Cat# 502928; RRID: AB_2561315
APC/Fire 750 anti-human CD49a	BioLegend	Cat# 328318; RRID: AB_2810495
Phycoerythrin (PE) anti-human CD366 (Tim-3)	BioLegend	Cat# 345006; RRID: AB_2116576
PE/Cyanine 5 anti-human CD62L	BioLegend	Cat# 304808; RRID: AB_314468
Peridinin-Chlorophyll-Protein (PerCP)/Cyanine 5.5 anti-mouse CD45	BioLegend	Cat# 103132; RRID: AB_893340
Fluorescein (FITC) anti-human CD103 (Integrin alphaE)	BioLegend	Cat# 350204; RRID: AB_10639865
Biotin anti-human CD103 (Integrin alphaE)	BioLegend	Cat# 350220; RRID: AB_2629646
APC-H7 anti-human CD8	BD Biosciences	Cat# 641409; RRID: AB_1645737
PE-CF594 anti-human CD197 (CCR7)	BD Biosciences	Cat# 562381; RRID: AB_11153301
PE-CF594 anti-human IL-2	BD Biosciences	Cat# 562384; RRID: AB_11154601
APC-H7 anti-human CD45	BD Biosciences	Cat# 560274; RRID: AB_1645480
PE anti-human RUNX3	BD Biosciences	Cat# 564814; RRID: AB_2738969
APC anti-human CD25	ThermoFisher Scientific	Cat# 17-0259-42; RRID: AB_1582219
PE/Cyanine 5.5 anti-human Granzyme B	ThermoFisher Scientific	Cat# GRB18; RRID: AB_2536541
APC anti-human TOX	Miltenyi Biotec	Cat# 130-118-335; RRID: AB_2751485
PE/Cyanine 7 anti-human CD223 (LAG-3)	eBioscience	Cat# 25-2239-42; RRID: AB_2573430
APC anti-FMC63 CAR19	ACROBiosytems	Cat# FM3-AY54P1
Biological samples		
Human Healthy Donor PBMC	Human Immunology Core, University of Pennsylvania	N/A
Chemicals, peptides, and recombinant proteins		
PE-conjugated Mesothelin Protein	AcroBiosystems	Cat# MSN-HP2H5
PSMA Protein, Human, Recombinant (His Tag), Biotinylated	Sino Biological	Cat# 15877-H07H-B
Recombinant Human TGF-beta 1 Protein	R&D Systems	Cat# 240-B-002
Recombinant Human Interleukin-2 (IL-2) Protein	R&D Systems	Cat# 202-IL-050
Human TGF-β1 Recombinant Protein	Cell Signaling Technology	Cat# 75362S
D-Luciferin	PerkinElmer	Cat# 122799
TRIzol	ThermoFisher Scientific	Cat# 15596026
Truecut™ Cas9 Protein v2	ThermoFisher Scientific	Cat# A36498
Matrigel Basement Membrane Matrix	Corning	Cat# 356234
Alt-R® CRISPR-Cas9 tracrRNA	Integrated DNA Technologies	Cat# 1072534

(*Continued on next page*)

Continued

REAGENT or RESOURCE	SOURCE	IDENTIFIER
Collagenase Type IV	STEMCELL Technologies	Cat# 07909
DNase I Solution	STEMCELL Technologies	Cat# 07900
123count eBeads™	ThermoFisher Scientific	Cat# 01-1234-42
AMPure Beads	Beckman Coulter	Cat# E6116
Dynabeads human T-activator CD3/CD28	ThermoFisher Scientific	Cat# 11131D
Critical commercial assays		
96-well RTCA E-plates	Agilent	Cat# 300601010
MycoAlert® Mycoplasma Detection Kit	Lonza	Cat# LT07-318
Pan T cell Isolation Kit, human	Miltenyi Biotec	Cat# 130-096-535
RNA Clean & Concentrator™ Kits	Zymo Research	Cat# R1015
P3 Primary Cell 4D-nucleofector Kit	Lonza	Cat# V4XP-3032
13-plex LEGENDplex™ Human CD8 Panel	BioLegend	Cat# 740267
LIVE/DEAD™ Fixable Aqua Dead Cell Stain Kit	ThermoFisher Scientific	Cat# L34957
Foxp3 Transcription Factor Staining Buffer Set	ThermoFisher Scientific	Cat# 00-5523-00
Chromium Next GEM Single Cell 5′ Kit v2	10X Genomics	Cat# PN-1000263
Dead Cell Removal Kit	Miltenyi Biotec	Cat# 130-090-101
Deposited data		
RNA- and ATAC-seq data	NCBI Gene expression omnibus (GEO)	GSE224866
Experimental models: Cell lines		
NALM6, clone G5	ATCC	CRL-3273
Capan-2	ATCC	HTB-80
AsPC-1	ATCC	CRL-1682
PC3	ATCC	CRL-1435
HEK 293T	ATCC	CRL-3216
EMMESO	Steven M. Albelda Lab	N/A
Experimental models: Organisms/strains		
NOD/SCID/IL-2Rγ-null (NSG) mice	University of Pennsylvania Stem Cell and Xenograft Core	N/A
Oligonucleotides		
Please see Table S3.	This study	N/A
Recombinant DNA		
pTRPE-RUNX3	Steven M. Albelda Lab	N/A
pTRPE-M5 (anti-mesothelin) CAR (4-1BB/CD3ζ)	Carl H. June Lab	N/A
pTRPE-SS1 (anti-mesothelin) CAR (4-1BB/CD3ζ)	Carl H. June Lab	N/A
pTRPE-PSMA CAR (4-1BB/CD3ζ)	Carl H. June Lab	N/A
pTRPE-CD19 CAR (4-1BB/CD3ζ)	Carl H. June Lab	N/A
Software and algorithms		
FlowJo v10	FlowJo, LLC	https://www.flowjo.com; RRID:SCR_008520
GraphPad Prism v9.1.0	GraphPad	https://www.graphpad.com; RRID:SCR_002798
RTCA 2.0	Agilent	https://www.agilent.com
Inference of CRISPR Edits (ICE) Tool	Synthego	https://ice.synthego.com
Cell Ranger v6.1.2	10X Genomics	https://support.10xgenomics.com/single-cell-gene-expression/software/pipelines/latest/using/tutorial_ct
Seurat v4.1.1	Satija Lab	https://github.com/satijalab/seurat
SCTransform (part of Seurat)	Christoph Hafemeister, Rahul Satija	https://github.com/ChristophH/sctransform

(*Continued on next page*)

Continued

REAGENT or RESOURCE	SOURCE	IDENTIFIER
Functions within Seurat (SelectIntegrationFeatures, PrepSCTIntegration, FindIntegrationAnchors, IntegrateData, RunPCA, FindNeighbors, FindClusters, runUMAP, FindMarkers, FindAllMarkers, AddModuleScore)	Satija Lab	https://satijalab.org/seurat/reference/index.html
Cutadapt	Marcel Martin	https://github.com/marcelm/cutadapt
Bowtie2	Ben Langmead, Cole Trapnell, Mihai Pop, Steven Salzberg	https://github.com/BenLangmead/bowtie2
removeChrom	John M. Gaspar	https://github.com/jsh58/harvard/blob/master/removeChrom.py
Samtools	Heng Li, Bob Handsaker, and colleagues	https://github.com/samtools/samtools
The Integrative Genome Viewer (IGV)	Broad Institute	https://github.com/igvteam/igv
MACS2	Tao Liu and colleagues	https://github.com/taoliu/MACS
ENCODE blacklisted regions	Anshul Kundaje Lab	https://sites.google.com/site/anshulkundaje/projects/blacklists
findMotifsGenome script from HOMER	Chris Benner and colleagues	http://homer.ucsd.edu/homer/ngs/peakMotifs.html
edgeR v3.34.0	Gordon Smyth, Yunshun Chen, Matthew Ritchie, and colleagues	https://bioconductor.org/packages/release/bioc/html/edgeR.html
enrichr	Ma'ayan Lab	https://maayanlab.cloud/Enrichr
GSEABase	Martin Morgan, Dan Tenenbaum, and colleagues	https://github.com/Bioconductor/GSEABase
kallisto v0.46.0	Páll Melsted, Lior Pachter, and colleagues	https://github.com/pachterlab/kallisto
tximport 1.24.0	Michael Love, Charlotte Soneson, Mark Robinson, and colleagues	https://github.com/mikelove/tximport

RESOURCE AVAILABILITY

Lead contact

Additional information and inquiries regarding resources and reagents should be directed to the lead contact, Dr. Joseph Fraietta (jfrai@upenn.edu), who will fulfill these requests.

Materials availability

Requests for materials should be directed to the Penn Center for Innovation (pciinfo@pci.upenn.edu). All requests will be promptly reviewed to determine if they involve any intellectual property considerations. Materials eligible for sharing will be released following the execution of a material transfer agreement.

Data and code availability

- The sequencing data reported in this paper is deposited in the Gene Expression Omnibus (GEO) database with accession number GSE224866. The data is available for public access and download from the GEO database, with no restrictions on its use or redistribution.
- No original code is featured in this paper.
- Any additional information required to reanalyze the data reported in this work paper is available from the lead contact upon request.

EXPERIMENTAL MODEL AND SUBJECT DETAILS

Cell lines

The NALM6 B-cell acute lymphoblastic leukemia cell line, pancreatic ductal adenocarcinoma cell lines Capan-2 and AsPC-1 expressing mesothelin, the PC3 prostatic adenocarcinoma cell line, and HEK 293T cells were acquired from the American Type Culture Collection (ATCC). PC3 cells were modified to express PSMA (PC3-PSMA), and both PC3-PSMA and NALM6 cells were engineered to express click beetle green luciferase and green fluorescent protein (CBG-GFP). A human mesothelioma cell line, EMP (parental), derived from a patient's tumor in March 2010, was also used. EMP was altered to express human mesothelin (EMMESO) as it does

not endogenously express it. Antigen expression was confirmed in these cell lines before functional assays. Capan-2, PC3-PSMA, and HEK 293T cells were cultured in D10 media with Dulbecco's Modified Eagle Medium (DMEM, Gibco), supplemented with high glucose, GlutaMAX, 10% fetal bovine serum (FBS, Gibco), and 1% penicillin/streptomycin. NALM6, AsPC-1, and EMMESO cells were maintained in Roswell Park Memorial Institute (RPMI) 1640 media containing 10% FBS and 1% streptomycin/penicillin (R10). The University of Arizona Genetics Core authenticated all cell lines used in this study, and mycoplasma contamination was tested using the MycoAlert Mycoplasma Detection kit (Lonza) according to the manufacturer's protocol.

Primary human T-cells

For the generation of CAR T-cells, mononuclear cells from peripheral blood (PBMC) were acquired through leukapheresis from healthy volunteers. These cells were obtained from the Human Immunology Core at the University of Pennsylvania, with the approval of the university's Institutional Review Board. Study participants provided written informed consent, in compliance with the Declaration of Helsinki, the International Conference on Harmonization's Good Clinical Practice guidelines, and the United States Common Rule.

Mice

Animal studies were conducted using both male and female NOD/SCID/IL-2Rγ-null (NSG) mice aged between eight and twelve weeks, obtained from the University of Pennsylvania Stem Cell and Xenograft Core. These experiments were carried out under a protocol approved by the Institutional Animal Care and Use Committee. This ensured that all experiments involving the mice adhered to the highest ethical standards and guidelines for animal care and use in scientific research. The mice were housed in a pathogen-free environment, subjected to a 12-h light/dark cycle, and maintained at a consistent temperature of 21 $\pm$ 2°C with 60 $\pm$ 20% relative humidity. The animals were given unrestricted access to acidified water and sterilized food.

METHOD DETAILS

Lentivirus production

Lentivirus manufacturing was carried out previously described.[42] Briefly, the pTRPE lentiviral transfer plasmid was modified to facilitate expression of the human RUNX3 transcription factor or second-generation CAR constructs comprised of extracellular anti-mesothelin (M5 and SS1), -PSMA or anti-CD19 single chain variable fragments, CD8a hinge/transmembrane domains, and 4-1BB and CD3ζ cytoplasmic signaling modules. At 70–80% confluency, low passage HEK 293T cells were transfected with lentiviral transfer plasmid and packaging vectors using Lipofectamine 2000 (ThermoFisher Scientific). At 24- and 48-h post-transfection, lentivirus supernatant was harvested, followed by concentration using high-speed ultracentrifugation. After removal of supernatant, R10 media was added for resuspension of viral pellets and stored at stored at -80°C.

T-cell culture and lentiviral transduction

PBMCs were isolated from buffy coats and cryopreserved at 4×10^7 cells per vial. Cryopreserved PBMCs were thawed, and T-cell purification was carried out using the Pan T Cell Isolation Kit according to the manufacturer's instructions (Miltenyi Biotec). For CAR-T_{CONV} manufacturing, T-cells were activated with CD3/CD28 Dynabeads (ThermoFisher Scientific) at a bead to cell ratio of 3:1 for three days in T-cell OpTmizer CTS SFM media (Gibco) supplemented with 5% human AB serum and 100U/mL human IL-2 (T-cell media). At 24-h post-T-cell activation, T-cells were transduced with the above lentiviral vectors at a multiplicity of infection (MOI) of three. T-cell media was added to cultures every two days, and on day nine, CAR T-cells were cryopreserved in T-cell media supplemented with 20% human AB serum and 10% dimethyl sulfoxide. For CAR-T_{RM} production, T-cell culture media was supplemented with 2 ng/mL of TGF-β (R&D Systems or Cell Signaling Technology) in addition to IL-2, and the CAR T-cell engineering process was carried out as specified above.

Gene editing using CRISPR/Cas9

At three days following T-cell activation, CD3/CD28 Dynabeads were magnetically removed. T-cells were washed with phosphate-buffered saline (PBS), and electroporation was carried out using the P3 primary cell 4D-nucleofector kit (Lonza). Ribonucleoprotein (RNP) complexes were generated by preincubating 12 μg TrueCut S. Cas9 (ThermoFisher Scientific), 0.2 nmol Alt-R tracrRNA (*trans*-activating CRISPR RNA), and crRNA (crispr RNA) (Integrated DNA Technologies) for 10 min. Three million CAR T-cells resuspended in P3 buffer were added to the appropriate RNP complexes, followed by transfer to nucleocuvette strips for electroporation using the 4D-Nucleofactor (Lonza, protocol EO-115). After electroporation, CAR T-cells were maintained in T-cell media supplemented with or without 2 ng/mL of TGF-β. Three days post-electroporation, CAR T-cells were collected for genomic DNA isolation. Target regions flanking double-strand brake sites were amplified by polymerase chain reaction (PCR) for Sanger sequencing. Editing efficiencies were determined by Inference of CRISPR Edits (ICE) analysis.

Flow cytometry

For flow cytometric characterizations, CAR T-cells were first stained with LIVE/DEAD Fixable Aqua Dead Cell Stain Kit (ThermoFisher Scientific) in PBS. Samples were subsequently washed and incubated with antibodies diluted in FACS buffer (PBS +2% FBS). Expression of anti-mesothelin CARs and the anti-CD19 CAR was measured using a PE-conjugated mesothelin protein and an

APC-conjugated anti-FMC63 idiotype antibody, respectively. PSMA CAR expression was assessed using a biotinylated recombinant human PSMA protein sourced from Sino Biological, followed by a secondary stain with APC-conjugated streptavidin. Additional surface proteins were stained using the following antibodies: BV 421 anti-human CD279 (PD-1), BV 570 anti-human CD45RO, BV 650 anti-human CD8a, BV 785 anti-human CD4, BV 570 anti-human CD127 (IL-7Ralpha), PE anti-human CD366 (Tim-3), PE/Cyanine 5 anti-human CD62L, PerCP/Cyanine 5.5 anti-mouse CD45, FITC anti-human CD103 (Integrin alphaE), APC-H7 anti-human CD8, PE-CF594 anti-human CD197 (CCR7), APC-H7 anti-human CD45, APC anti-human CD25, APC/Fire 750 anti-human CD49a, PE/Cyanine 7 anti-human CD223 (LAG-3), and/or BV 711 anti-human CD39. For intracellular protein staining, cells were first fixed and permeabilized using the Foxp3 Transcription Factor Staining Buffer Set (ThermoFisher Scientific), followed by staining with the following antibodies: PE-CF594 anti-human IL-2, BV 570 anti-human IFN-gamma, AF 700 anti-human TNF-alpha, BV 421 anti-human Perforin, APC anti-human Perforin, PE anti-human RUNX3, PE/Cyanine 5.5 anti-human Granzyme B, and/or APC anti-human TOX. Fluorescence intensity for each sample was measured using an LSRII Fortessa cytometer (BD Biosciences), and analysis was performed with FlowJo software v10 (FlowJo, LLC).

In vitro restimulation assay

The resident memory phenotype of CAR T-cells was assessed using an *in vitro* restimulation assay. Briefly, 5×10^5 irradiated AsPC-1 cells were seeded a day before coincubation with CAR T-cells. M5 CAR T-cells were magnetically isolated using anti-mesothelin-coated beads (ACROBiosystems). The isolated 1×10^6 CAR T-cells were then added to AsPC-1 cells at an effector to target ratio of 2:1. After 18-h of coincubation, supernatant was collected for cytokine measurements using the 13-plex LEGENDplex human CD8 panel (BioLegend). On every fifth day following tumor cell challenge, CAR T-cells were harvested for immunophenotyping, and 1×10^6 viable CAR T-cells were transferred into plates containing AsPC-1 cells to facilitate chronic stimulation.

Cytotoxicity assay

The xCELLigence system (ACEA Biosciences Inc.) was used to monitor that cytolytic capacity of anti-M5 CAR-T_{CONV} and CAR-T_{RM} cells. For this assay, 4×10^4 AsPC-1 cells were seeded in E-Plate VIEW 96 PET microwell plates, and after 24-h, 2×10^4 M5 CAR T-cells or irrelevant CD19 CAR T-cells were added at an effector to target ratio of 1:2. Tween 20 was used as a positive control for full cell lysis. The real-time cell index was monitored in 20-min intervals over seven days, and the degree of CAR T-cell-mediated cytotoxic activity was calculated using the normalized cell index and percent cytolysis.

Mouse xenograft studies

To assess the *in vivo* antitumor potency of M5 CAR-T_{CONV} and CAR-T_{RM} cells in solid tumor indications, 4×10^6 AsPC-1 cells or 5×10^6 Capan-2 cells were premixed with Matrigel (Corning) and subcutaneously inoculated in the right flanks of 6- to 8-week-old NSG mice. For the AsPC-1 model, 3×10^5 M5 CAR T-cells were intravenously infused on day thirty-two following tumor engraftment. For Capan-2 xenograft experiments, 1×10^5 CAR T-cells were intravenously given to Capan-2-bearing mice on day twenty-nine. To examine the role of the resident memory population in mediating CAR-T_{RM} cell antitumor responses, the $CD103^+$ population in CAR-T_{RM} products was magnetically depleted using biotinylated anti-human CD103 antibody and anti-biotin microbeads (Miltenyi Biotec). Following isolation, $CD103^+$cell-depleted CAR-T_{RM} cells were administered to mice. Longitudinal tumor growth was monitored using caliper measurements (tumor volume = (length $\times$ $width^2$)/2) in AsPC-1 and Capan-2 models. To assess the trafficking of CAR T-cells, the M5 CAR-T_{CONV} and CAR-T_{RM} cells were labeled with 320 μg/mL IVISense DiR 750 fluorescent cell labeling dye (PerkinElmer) for 30 min. After washing the CAR T-cells twice with PBS, they were intravenously injected into the mice on day thirty-three post-Capan-2 engraftment. The migration of the CAR T-cells was monitored using the Xenogen IVIS Imaging System (PerkinElmer) with a 710 nm excitation and 760 nm emission filter.

To assess the immunophenotype of tumor-infiltrating CAR T-cells, Capan-2 tumors were harvested on day thirteen post-CAR-T cell injection and minced with a scalpel. Tumors were subsequently dissociated with 100 U/mL Collagenase Type IV (STEMCELL Technologies) and 0.25 mg/mL DNase I (STEMCELL Technologies) for 30 min at 37°C. Tumor-infiltrating CAR T-cells were then re-activated with 50 ng/mL of phorbol 12-myristate 13-acetate 1210 (PMA) and 1 μg/mL ionomycin in the presence of 5 μg/mL Brefeldin A for 6-h. Expression of effector cytokines and cytotoxic proteins were assessed by flow cytometry. To assess the antitumor efficacy of SS1 CAR T-cells, NSG mice were injected with EMMESO mesothelin-expressing mesothelioma cells. When tumor volume reached a size of ~120 mm^3, mice were infused with a single dose of 10^7 CAR T-cells.

For the NALM6 B-cell leukemia model, NSG mice were engrafted with 10^6 NALM6 cells intravenously. On day seven post-tumor injection, anti-CD19 CAR-T_{CONV}, CAR-T_{RM} cells, or irrelevant PSMA CAR T-cells (negative control), were infused. Longitudinal tumor growth was assessed weekly using bioluminescent imaging with the Xenogen IVIS Imaging System. On day nineteen after tumor injection, peripheral blood was collected from mice to evaluate CAR T-cell expansion capacity and differentiation phenotype. The number of human peripheral blood T-cells was measured using 123count eBeads (ThermoFisher Scientific), and surface memory markers were stained for flow cytometric analysis according to the above methods.

In the intraosseous PC3-PSMA model, 2×10^5 PC3-PSMA cells were intrafemorally transplanted into male NSG mice. After 21 days, the mice received an intravenous infusion of 1×10^5 anti-PSMA CAR-T_{CONV} or -CAR-T_{RM} cells. Tumor burden was assessed by administering an intraperitoneal injection of luciferin to the mice, followed by quantifying bioluminescence using the Xenogen IVIS Imaging System.

Bulk RNA-seq

Anti-mesothelin M5 CAR-T_{CONV} and CAR-T_{RM} cells were harvested after nine days of *in vitro* expansion. $CD8^+$ CAR T-cells were magnetically isolated using anti-mesothelin-coated beads (ACROBiosystems) and anti-CD8 microbeads (Miltenyi Biotec), followed by resuspension in 500μL of TRIzol (Invitrogen). Total RNA was prepared using RNA Clean & Concentrator kits (Zymo Research) following the manufacturer's instructions. Transcriptome sequencing was performed by Novogene using the NovaSeq 6000 system (Illumina, 150bp paired end reads). Paired-end reads were pseudoaligned to the human genome (GRCh38) using kallisto v0.46.0, and count estimates at the gene level were summarized using tximport 1.24.0.

Differential gene expression analyses between CAR-T_{RM} and CAR-T_{CONV} cells was conducted using edgeR v3.34.0. Briefly, filtered RNA-seq data was normalized using a TMM method (Trimmed Mean of M-values) and logarithmically transformed into counts per million (cpm). Generalized linear models were used to determine differential expression in a paired design using edgeR. Gene set enrichment analysis (GSEA) was conducted using enrichr and GSEABase on the following gene sets: resident-memory gene sets[48] (Table S1: genes differentially expressed between $CD69^+CD103^+$ and $CD69^-CD103^-CD8^+$ T-cells, adjusted p value <0.05 and log2FC $\geq$ 1), hypoxia and migration gene sets (MSigDB C2), and response to ICB signature.[49]

Single-cell RNA sequencing

For scRNA-seq, dead cells were eliminated using the Dead Cell Removal Kit (Miltenyi Biotec). Mesothelin-directed M5 CAR-T_{CONV} and -T_{RM} cells were magnetically isolated using anti-mesothelin-coated beads, as described above. After isolation, T-cell viability and quantity were evaluated using trypan blue exclusion and cells were resuspended in PBS containing 0.04% BSA. Approximately 20,000 cells were loaded per reaction to capture ~10,000 cells for scRNA-seq library preparation using the Chromium Next GEM Single Cell 5′ Kit v2 (10X Genomics) according to manufacturer's protocol. Sequencing was performed on a NovaSeq 6000 instrument at a depth of >20,000 reads per cell.

Raw read files were processed and aligned to the human reference genome (GRCh38) using Cell Ranger 6.1.2. Expression data were then analyzed in R using Seurat version 4.1.1. Poor quality cells with more than 10% mitochondrial reads were eliminated, and cells that express less than 1,000 genes or more than 7,000 genes were also eliminated. After cell filtration, 12,230 cells were obtained for subsequent analysis. Analyses were carried out using various additional packages of reproducible R code. Individual data sets were normalized via regularized negative binomial regression using SCTransform. Normalized expression datasets from CAR-T_{CONV} and CAR-T_{RM} samples were integrated with SelectIntegrationFeatures, PrepSCTIntegration, FindIntegrationAnchors, and IntegrateData commands. Principal component analysis was carried out on scaled data using RunPCA, followed by clustering of cells using FindNeighbors, and FindClusters. UMAP embedding was done with the runUMAP function. Differential gene expression analyses between CD8 clusters or CAR T-cell samples were performed using the FindMarkers and FindAllMarkers commands. We queried expression datasets for the expression of resident-memory[48] and 'stemness'-related (GSE83978) gene signatures and calculated module scores using AddModuleScore.

ATAC-seq analysis

Anti-mesothelin M5 CAR-T_{CONV} and CAR-T_{RM} cells were harvested after nine days of *in vitro* expansion. CAR T-cells were magnetically isolated according to the methods described above. After elimination of dead cells, 100,000 $CD8^+$ CAR T-cells were cryopreserved. Library preparation was performed by Novogene as follows: a reaction mixture consisting of Tn5 transposase and equimolar adapter1 and adapter 2 was added to nuclei pellets and incubated at 37°C for 30 min. The library was enriched using PCR, and purification of final libraries was carried out using AMPure beads (Beckman Coulter). Paired-end sequencing (150bp reads) was conducted on a NovaSeq 6000 instrument.

Cutadapt was used to trim FASTQ files of adapter contamination. Reads were aligned to the hg19 reference genome using Bowtie2, retaining only properly aligned and paired reads from 10 to 1000 base pairs. Mitochondrial reads were then eliminated using removeChrom. Aligned reads were converted to BAM files and sorted with samtools, and Picard was used to remove PCR duplicates. BAM files were indexed using samtools to display tracks in the Integrative Genome Viewer (IGV). MACS2 was used to call peaks with an FDR q-value cutoff of 0.01. The R package Diffbind was used to remove ENCODE blacklisted regions, then to identify peaks differentially opened between the CAR-T_{CONV} and -T_{RM} populations. The findMotifsGenome script from HOMER was implemented to map differentially opened peaks for occurrences of known transcription factor motifs.

Statistical analyses

Statistical tests between two groups were carried out using a two-tailed unpaired/paired Student's *t* *t*-test (for parametric data) or a Mann-Whitney U test (for non-parametric data). The Benjamini–Hochberg procedure was used to adjust p values for multiple comparisons testing following differential gene expression analyses. For statistic comparisons involving three or more groups, one- or two-way ANOVA tests were performed, followed by post-hoc testing for multiple comparisons. Mouse survival was assessed using the Log rank (Mantel-Cox) test. Statistical analyses were carried out using GraphPad Prism v9.1.0 (GraphPad), and p values <0.05 were considered significant. *p < 0.05, *p < 0.01, ***p < 0.001, ns: not significant.

Cell Reports Medicine, Volume *4*

Supplemental information

Tissue-resident memory CAR T cells with stem-like characteristics display enhanced efficacy against solid and liquid tumors

In-Young Jung, Estela Noguera-Ortega, Robert Bartoszek, Sierra M. Collins, Erik Williams, Megan Davis, Julie K. Jadlowsky, Gabriela Plesa, Donald L. Siegel, Anne Chew, Bruce L. Levine, Shelley L. Berger, Edmund K. Moon, Steven M. Albelda, and Joseph A. Fraietta

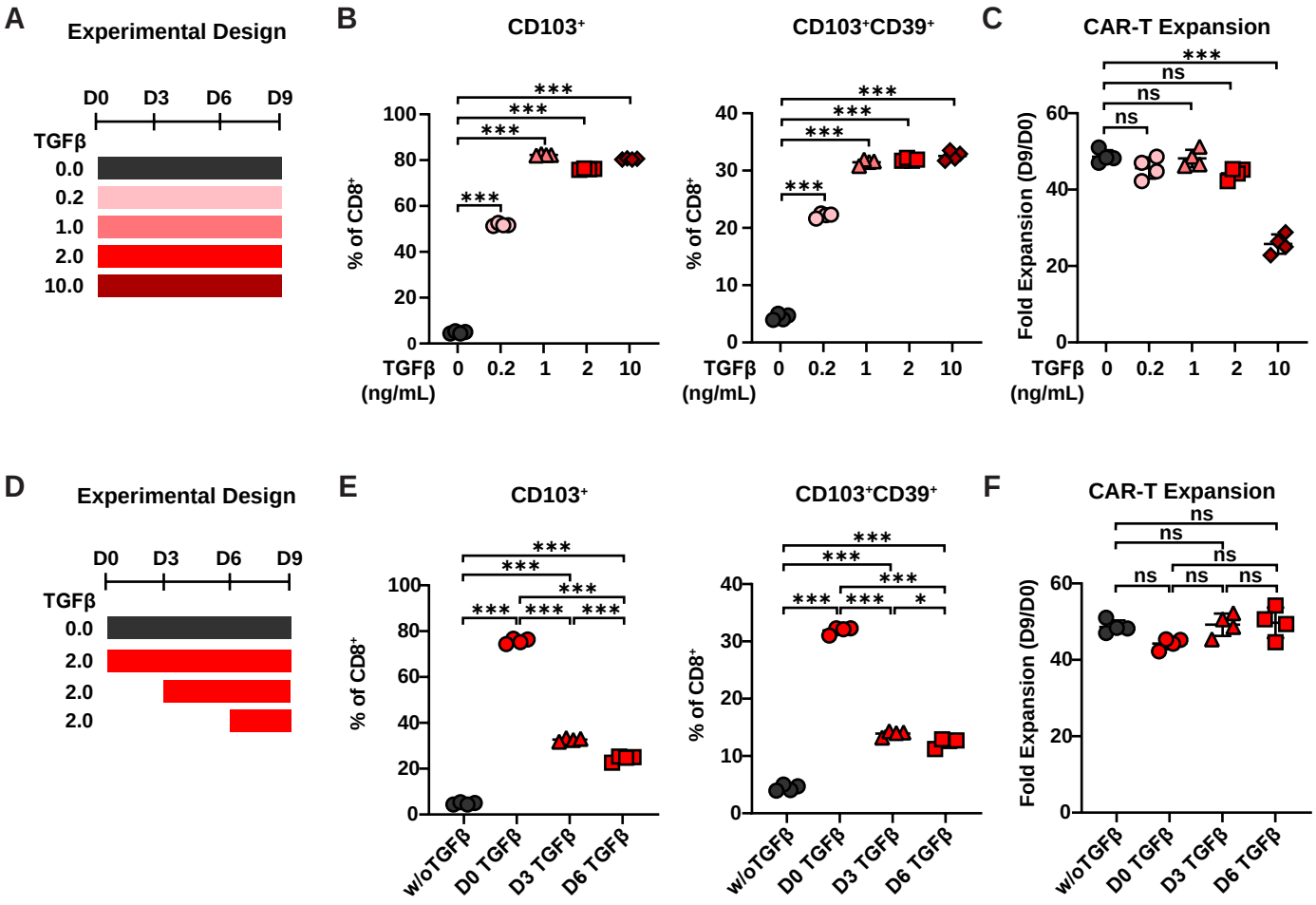
A
Experimental Design
D0
D3
D6
D9
TGFβ
0.0
0.2
1.0
2.0
10.0
B
CD103+
CD103+CD39+
% of CD8+
TGFβ (ng/mL)
0
0.2
1
2
10
***
C
CAR-T Expansion
Fold Expansion (D9/D0)
ns
D
Experimental Design
2.0
2.0
2.0
E
CD103+
CD103+CD39+
w/oTGFβ
D0 TGFβ
D3 TGFβ
D6 TGFβ
*
F
CAR-T Expansion

Supplementary Figure 1. Optimization of CAR-T_{RM} culture conditions. Related to Figure 1. (**A**) Schematic of optimizing TGF-β concentration. (**B**) Frequencies of $CD103^+$ and $CD103^+CD39^+$ $CD8^+$ CAR T-cells with 0, 0.2, 1, 2, 10 ng/mL TGF-β added during CAR T-cell manufacturing. (**C**) Fold CAR T-cell expansion during manufacturing with TGF-β concentration as indicated in panel **A**. (**D**) Schematic of optimizing duration of TGF-β exposure. (**E**) Frequencies of $CD103^+$ and $CD103^+CD39^+$ $CD8^+$ CAR T-cells with TGF-β added at different timepoints during CAR T-cell manufacturing. (**F**) Fold CAR T-cell expansion during manufacturing with TGF-β added on different timepoints as indicated in panel **D**. One-way ANOVA, $n = 4$ biological replicates. $*P < 0.05$, $*P < 0.01$, $***P < 0.001$, ns.: not significant.

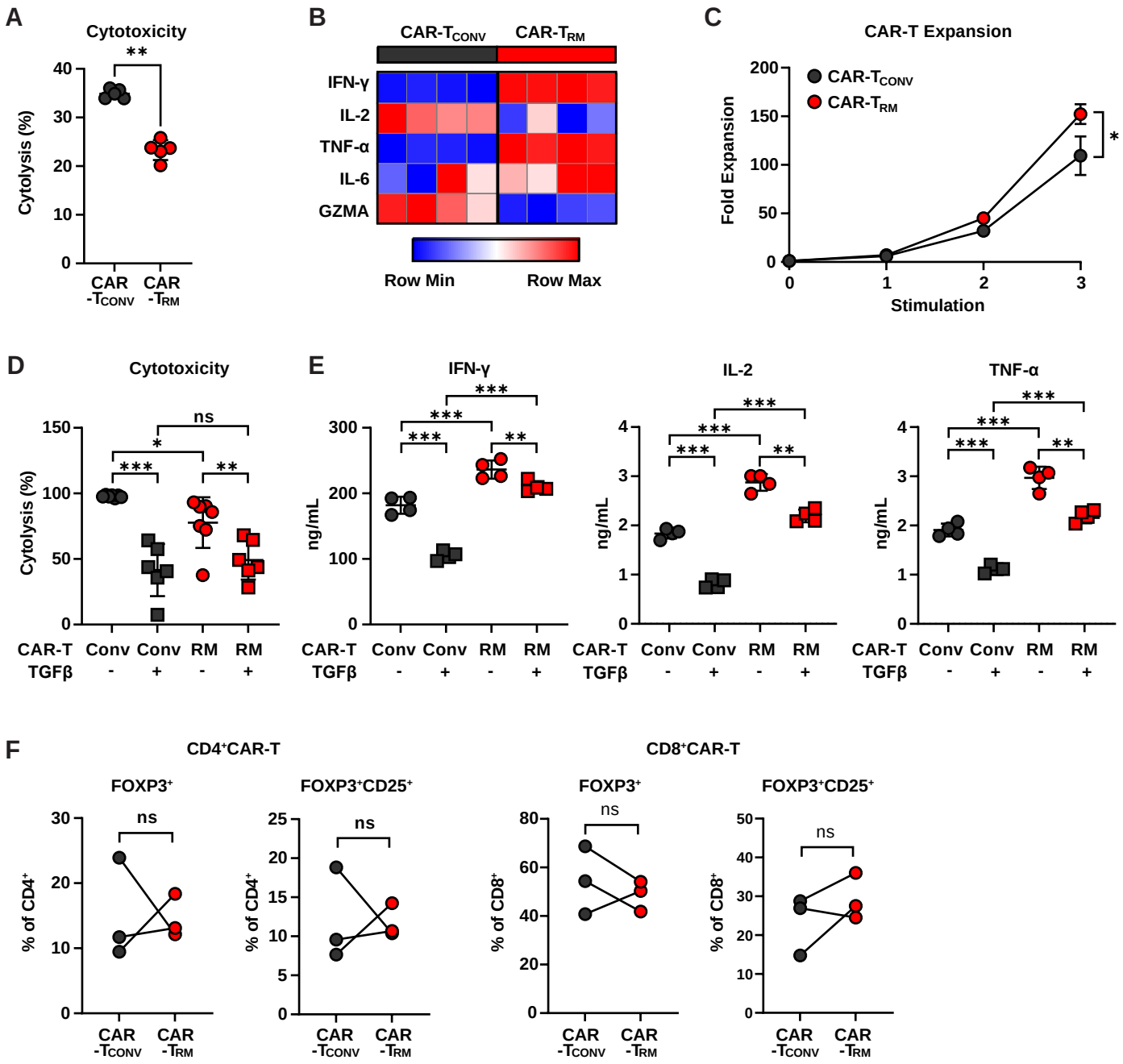
A
Cytotoxicity
Cytolysis (%)
CAR -TCONV
CAR -TRM
B
CAR-TCONV
CAR-TRM
IFN-γ
IL-2
TNF-α
IL-6
GZMA
Row Min
Row Max
C
CAR-T Expansion
CAR-TCONV
CAR-TRM
Fold Expansion
Stimulation
D
Cytotoxicity
Cytolysis (%)
CAR-T
TGFβ
Conv Conv RM RM
E
IFN-γ
IL-2
TNF-α
ng/mL
F
CD4+CAR-T
CD8+CAR-T
FOXP3+
FOXP3+CD25+
% of CD4+
% of CD8+
ns

Supplementary Figure 2. Characterization of CAR-T_{RM} cells. Related to Figure 1.

(**A**) M5 CAR T-cells were isolated after three consecutive tumor challenges and co-cultured with Capan-2 target cells at an effector to target ratio of 1:2. Cytotoxic capacity at 7-hours post- co-culture is shown (Mann-Whitney test, $n = 5$ biological replicates). (**B**) Cytokine production after a second challenge with AsPC1 tumor cells. (**C**) Fold CAR T-cell expansion during a restimulation assay (Mann-Whitney test, $n = 4$ biological replicates). Experiments in panels **B-C** were conducted using CAR T-cells manufactured from different healthy donors. Figures display representative results from one donor. (**D, E**) M5 CAR T-cells were incubated with Capan-2 target cells at an effector to target ratio of 1:3 in presence or absence of 2 ng/mL TGFβ. The experiments were performed using CAR T-cells generated from individual healthy donors/biological replicates. (**D**) Cytolytic activity of CAR T-cells 4-days post-coculture. (**E**) Effector cytokine production 24-hours after co-incubation (one-way ANOVA, $n = 4$ biological replicates). (**F**) Frequencies of $FOXP3^+$ and $FOXP3^+CD25^+$ CAR T-cells after manufacturing (paired *t*-test, $n = 3$ biological replicates). $*P < 0.05$, $*P < 0.01$, $***P < 0.001$, ns.: not significant.

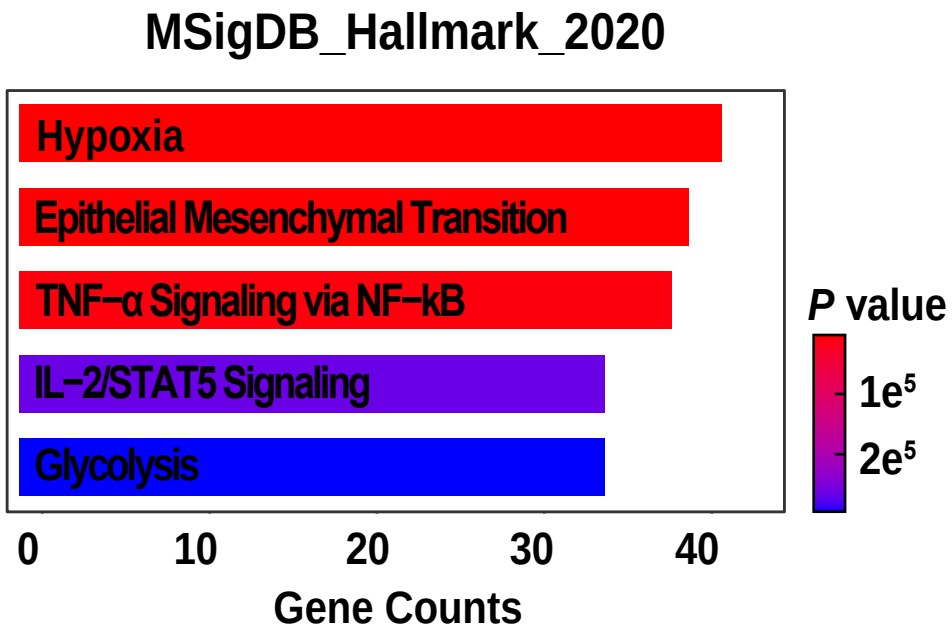
MSigDB_Hallmark_2020
Hypoxia
Epithelial Mesenchymal Transition
TNF−α Signaling via NF−kB
IL−2/STAT5 Signaling
Glycolysis
0
10
20
30
40
Gene Counts
P value
1e5
2e5

Supplementary Figure 3. Top pathways enriched in CAR-T_{RM} cells. Related to Figure 2.

Pathway analysis using Enrichr was carried out with genes upregulated in $CD8^+$ CAR-T_{RM} cells compared to $CD8^+$CAR-T_{CONV} cells (MSigDB_Hallmark_2020).

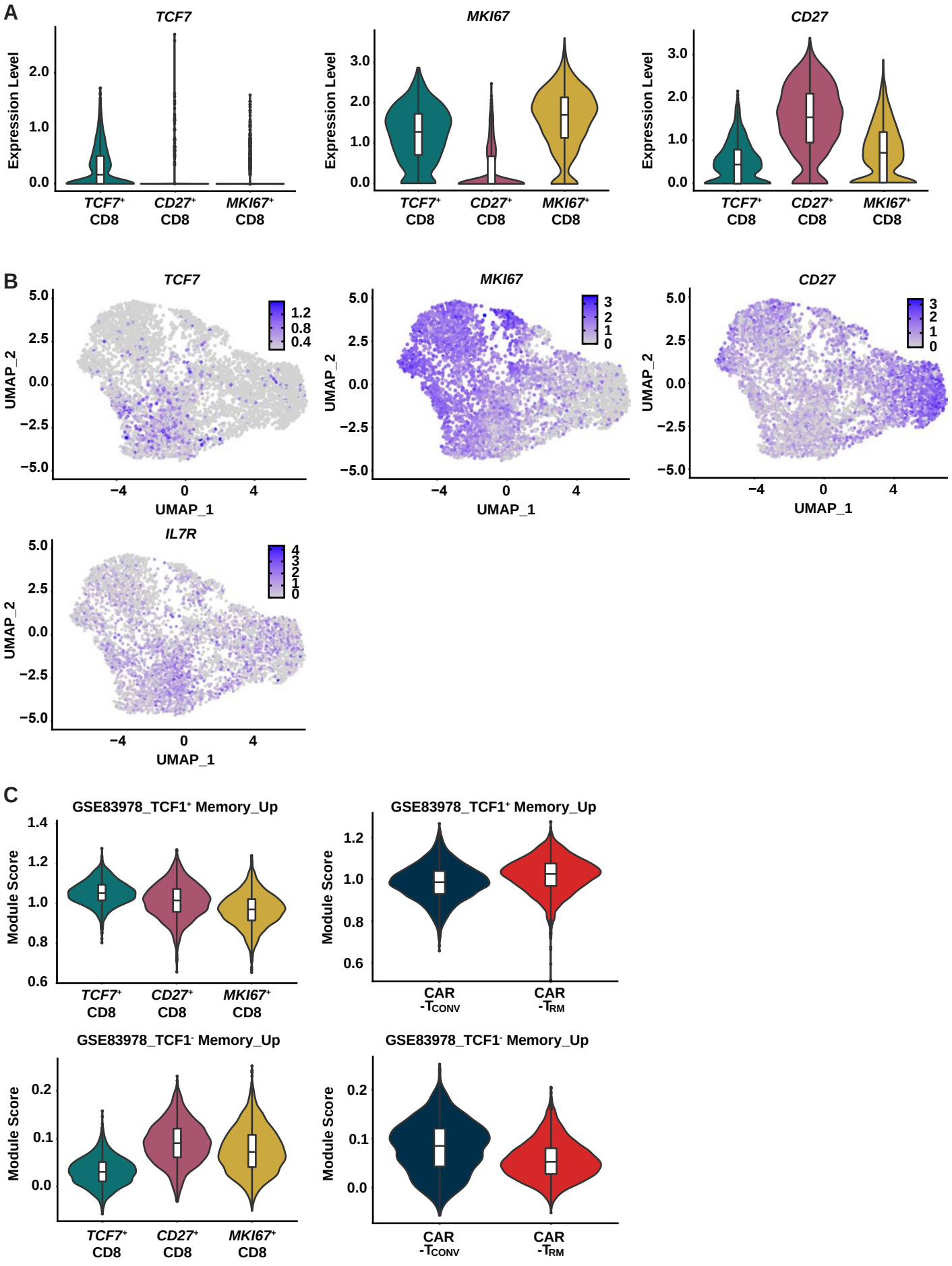
A
TCF7
MKI67
CD27
Expression Level
TCF7+ CD8
CD27+ CD8
MKI67+ CD8
B
TCF7
MKI67
CD27
IL7R
UMAP_1
UMAP_2
C
GSE83978_TCF1+ Memory_Up
GSE83978_TCF1- Memory_Up
Module Score
CAR -TCONV
CAR -TRM

Supplementary Figure 4. Single-cell gene expression analysis of CAR-T_{CONV} and CAR-T_{RM} cells. Related to Figure 3. (**A**) Violin plots displaying expression of cluster-defining markers in $CD8^+$ CAR T-cells. (**B**) UMAP plots illustrating expression levels of the same markers in the $CD8^+$ CAR T-cell population. (**C**) Module scores for 'stem-like' ($TCF1^+$ memory $CD8^+$ T-cells) and 'non-stem-like' ($TCF1^-$ memory $CD8^+$ T-cells) T-cell signatures were calculated for CD8 clusters and CAR T-cell samples (GSE83978).

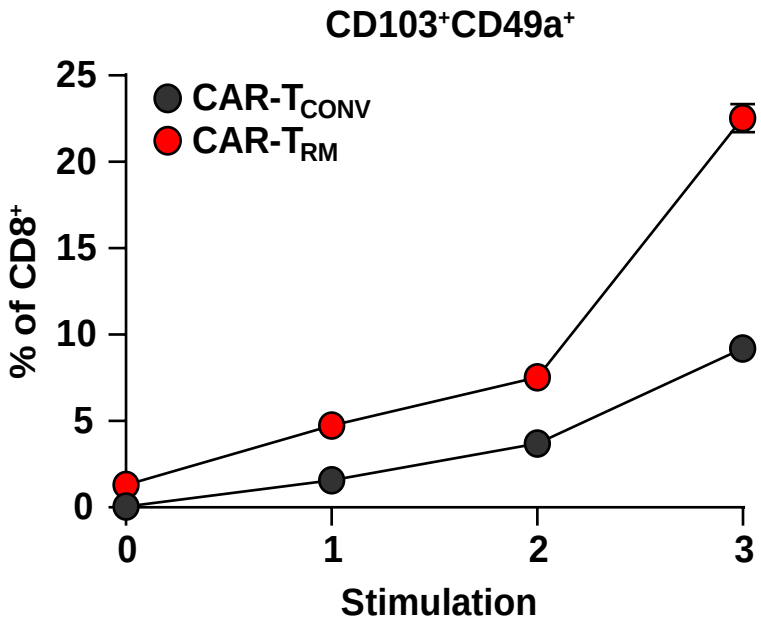
CD103+CD49a+
CAR-TCONV
CAR-TRM
% of CD8+
25
20
15
10
5
0
0
1
2
3
Stimulation

Supplementary Figure 5. Sustained resident memory phenotype of CAR-T_{RM} cells during chronic antigen stimulation. Related to Figure 4. Anti-mesothelin CAR T-cells were serially challenged with AsPC1 tumor cells, and frequencies of resident memory ($CD103^+CD49a^+CD8^+$) T-cells were assessed over time.

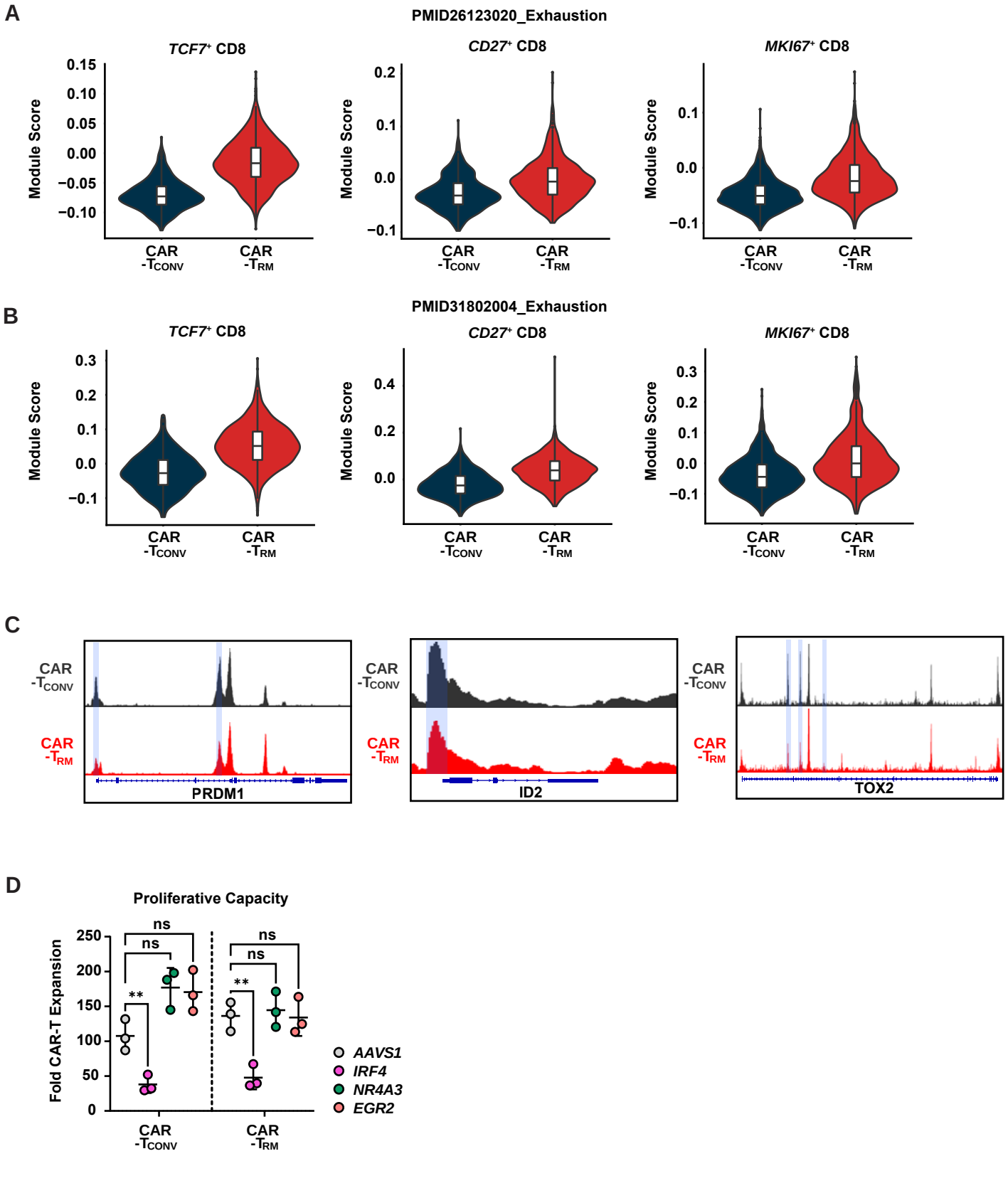
A
PMID26123020_Exhaustion
TCF7+ CD8
CD27+ CD8
MKI67+ CD8
Module Score
CAR -TCONV
CAR -TRM
B
PMID31802004_Exhaustion
C
PRDM1
ID2
TOX2
D
Proliferative Capacity
Fold CAR-T Expansion
ns
**
AAVS1
IRF4
NR4A3
EGR2

Supplementary Figure 6. Exhaustion features in CAR-T_{RM} cells. Related to Figure 5.

(**A, B**) Exhaustion scores are compared between CAR-T_{CONV} and CAR-T_{RM} in each $CD8^+$ T-cell cluster. (**A**) PMID26123020 (**B**) PMID31802004. (**C**) ATAC-seq tracks of *PRDM1*, *ID2*, and *TOX2*. Differentially accessible regions are highlighted in blue. (**D**) M5 CAR T-cells were serially challenged with AsPC1 cells at an E:T ratio of 2:1. Fold CAR T-cell expansion after the third round of antigen stimulation is shown (two-way ANOVA, $n = 3$ biological replicates). $^*P < 0.05$, $^*P < 0.01$, $^{***}P < 0.001$, ns.: not significant.

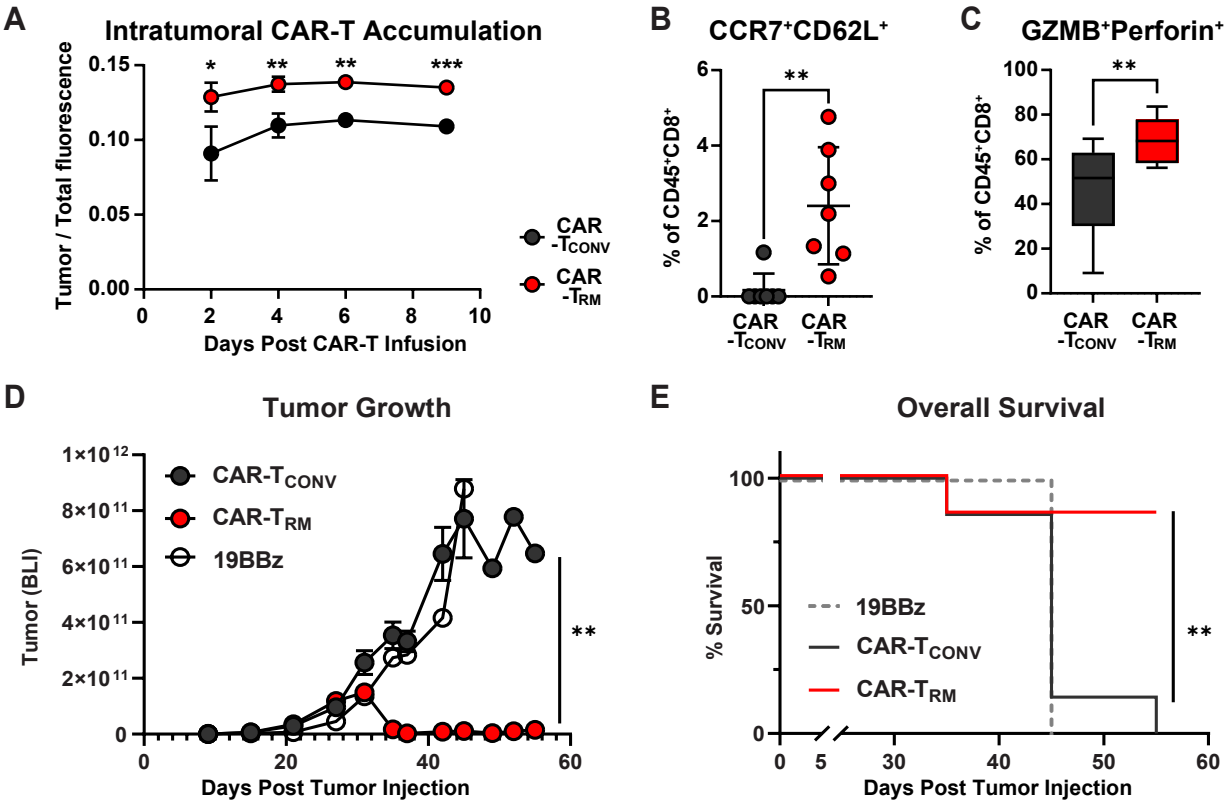
A
Intratumoral CAR-T Accumulation
Tumor / Total fluorescence
0.15
0.10
0.05
0.00
0
2
4
6
8
10
Days Post CAR-T Infusion
*
**
**
***
CAR -TCONV
CAR -TRM
B
CCR7+CD62L+
% of CD45+CD8+
6
4
2
0
**
CAR -TCONV
CAR -TRM
C
GZMB+Perforin+
% of CD45+CD8+
100
80
60
40
20
0
**
CAR -TCONV
CAR -TRM
D
Tumor Growth
Tumor (BLI)
1×10 12
8×10 11
6×10 11
4×10 11
2×10 11
0
0
20
40
60
Days Post Tumor Injection
CAR-TCONV
CAR-TRM
19BBz
**
E
Overall Survival
% Survival
100
50
0
0
5
30
40
50
60
Days Post Tumor Injection
19BBz
CAR-TCONV
CAR-TRM
**

Supplementary Figure 7. CAR-T_{RM} cell immunophenotype and antitumor efficacy in pancreatic and prostate cancer models. Related to Figure 6. (**A-C**) Capan-2 pancreatic cancer xenograft model: (**A**) NSG mice engrafted with 4×10^6 Capan-2 cells received M5 CAR-T_{CONV} and CAR-T_{RM} cells labeled with near-infrared (NIR) fluorescent dye intravenously on day 33 post-engraftment. NIR intensity was monitored over time (Unpaired *t*-test, $n = 3$ biological replicates). (**B**) Frequencies of $hCD45^+CD8^+$ cells in tumors expressing CCR7 and CD62L are shown (Mann-Whitney test, $n = 7$ biological replicates). (**C**) Tumor-infiltrating CAR T-cells were reactivated with phorbol 12-myristate 13-acetate and ionomycin, followed by measurement of effector molecule elaboration (Mann-Whitney test, $n = 12$ biological replicates). (**D-E**) Intraosseous PC3-PSMA prostate tumor model: (**D**) Male NSG mice intrafemorally engrafted with 2×10^5 PC3-PSMA cells received 1×10^5 anti-PSMA CAR-T_{CONV} or CAR-T_{RM} cells, or control CD19-targeting CAR T-cells (19BBz) intravenously on day 21 post-implantation ($n = 7$ biological replicates per group). Tumor burden was assessed by bioluminescent imaging after intraperitoneal injection of luciferin and quantification with the Xenogen IVIS Imaging System (one-way ANOVA). (**E**) Kaplan-Meier survival curves show prolonged survival in the CAR-T_{RM} group compared to CAR-T_{CONV} (Log-rank test). $^*P < 0.05$, $^{**}P < 0.01$, $^{***}P < 0.001$, ns: not significant.